Petrology and geochemistry of crustally contaminated komatiitic basalts from the Vetreny Belt, southeastern Baltic Shield: Evidence for an early Proterozoic mantle plume beneath ri...

Article *in* Geochimica et Cosmochimica Acta · March 1997

DOI: 10.1016/S0016-7037(96)00410-3

CITATIONS
205

READS
182

7 authors, including:

Igor S. Puchtel
University of Maryland, College Park
159 PUBLICATIONS **5,212** CITATIONS
SEE PROFILE

Karsten M. Haase
Friedrich-Alexander-University of Erlangen-Nürnberg
193 PUBLICATIONS **3,875** CITATIONS
SEE PROFILE

Albrecht W. Hofmann
Max Planck Institute for Chemistry
329 PUBLICATIONS **37,804** CITATIONS
SEE PROFILE

Catherine Chauvel
CNRS, IPGP
227 PUBLICATIONS **9,048** CITATIONS
SEE PROFILE

Pergamon

Geochimica et Cosmochimica Acta, Vol. 61, No. 6, pp. 1205–1222, 1997

0016-7037/97 $17.00 + .00

PII S0016-7037(96)00410-3

Petrology and geochemistry of crustally contaminated komatiitic basalts from the Vetreny Belt, southeastern Baltic Shield: Evidence for an early Proterozoic mantle plume beneath rifted Archean continental lithosphere

I. S. PUCHTEL,[1] K. M. HAASE,[1] A. W. HOFMANN,[1] C. CHAUVEL,[2] V. S. KULIKOV,[3] C.-D. GARBE-SCHÖNBERG,[4] and A. A. NEMCHIN[5]

[1]Max-Planck-Institut für Chemie, D-55020 Mainz, Germany
[2]Géosciences UPR 4661, CNRS, Université de Rennes I, F-35042 Rennes Cedex, France
[3]Institute of Geology, Karelian Research Center RAS, Pushkinskaya Str. 11, 185610 Petrozavodsk, Russia
[4]Geologisch-Paläontologisches Institut, Universität Kiel, 24118 Kiel, Germany
[5]School of Applied Geology, Curtin University of Technology Perth, Perth 6001, Australia

(*Received June* 27, 1996; *accepted in revised form December* 2, 1996)

Abstract—New isotope and trace element data are presented for komatiitic basalts and a related peridotite Vinela Dike from the large Vetreny Belt in the southeastern Baltic Shield. The MgO contents of the erupted and intruded magmas are inferred to increase from 13 to 17% towards the center of the belt, which implies the respective increase in liquidus temperatures from 1370 to 1440°C. The elevated liquidus temperatures suggest that the source of the komatiite magmas had a substantially higher potential temperature (1630°C) than the ambient mantle (1480°C) and are regarded as evidence for the existence of a mantle plume underlying the region at ~2.45 Ga. Parental magmas to the lavas and the Vinela Dike were shown to have komatiite composition and were derived from a long-term LREE-depleted mantle source with $\epsilon Nd(T)$ of ca. +2.6. The evolution of these magmas en route to the surface was mainly controlled by 4–15% contamination with older felsic crustal rocks, which resulted in substantial changes in incompatible trace element and isotope ratios. The obtained Sm-Nd internal isochron ages of 2449 ± 35 and 2410 ± 34 Ma for the lavas, 2430 ± 174 Ma for the Vinela Dike, and a whole-rock Pb-Pb age of 2424 ± 178 Ma for the lavas together with a U-Pb zircon age of 2437 ± 3 Ma are identical to the reported U-Pb zircon and baddeleyite ages for numerous mafic-ultramafic layered intrusions in central and northern Karelia. From their chemical and isotope similarities, it is likely that these rocks had allied parental magmas. These magmas may have been emplaced in a continental rift setting during the interaction of a mantle plume and continental crust. Impinging of a plume head beneath the continental lithosphere resulted in its thinning, stretching, and rifting but failed to open a new ocean. This extensive magmatic event was responsible for a substantial contribution of early Proterozoic juvenile material to the Archean continental crust in the Baltic Shield.

1. INTRODUCTION

During the past decade, substantial progress has been made in understanding the origin and growth of the continental crust. However, the location and mechanisms of initial extraction of the primitive crust from the mantle, and the processes by which this crust is converted into the continental crust that presently exists, are still not well understood. Recently, Abbott and Mooney (1995) have suggested that the distribution of continental crustal thicknesses is most consistent with the original production of the crust by mantle plumes and hotspots. Archaean and early Proterozoic granite-greenstone belts are among the most ancient fragments of Earth's crust. Several hypotheses have been proposed to explain the development of these enigmatic remnants of the distant geologic past. Accretion of oceanic plateaus formed by mantle plumes impinging beneath oceanic lithosphere explains unusually wide, long greenstone belts with uncontaminated komatiites, e.g., Abitibi belt (Desrochers et al., 1993). The accretion of ocean island chains may explain the occurrence of relatively small stacked greenstone belts containing komatiites (Hoffman, 1990), while the accretion of island arcs and back-arc basins could have explained bimodal volcanic rocks with deep-sea sedimentary sequences (Hoffman, 1990; Kimura et al., 1993). Continental plume volcanism explains the presence of crustally-contaminated komatiites with older detrital zircons (Compston et al., 1986). Narrow greenstone belts with intercalated mid-ocean ridge-like basalts (MORB) and arc-like volcanic rocks, which are juxtaposed with TTG-gneisses, may result from magmatism associated with the subduction of a mid-ocean ridge fed by a hotspot (Abbott, 1996). In addition to the lateral accretion of the crustal material, the continental crust may also grow through eruption of continental flood basalts and the intrusion of magmas in continental intraplate regions due to rifting initiated by impingement of mantle plumes upon the base of the continental lithosphere (McKenzie and Bickle, 1988; Arndt and Goldstein, 1989; Richards et al., 1989; Farnetani and Richards, 1994; White and McKenzie, 1995).

In this paper, we report new data on the geochemical and isotope compositions of high-magnesian lavas from the early Proterozoic Vetreny Belt in the southeastern Baltic Shield. We develop a model for the origin and evolution of these magmas and place some constraints on the tectonic setting of their emplacement.

2. GEOLOGICAL BACKGROUND

In the southeastern Baltic Shield, three large early Precambrian lithotectonic units are juxtaposed, comprising an Archean amphibolite-gneiss-migmatite and granite-greenstone

unit and a Lower Proterozoic volcanic-sedimentary unit. The Archean units are volumetrically dominant. They constitute the Karelian granite-greenstone terrane, which occupies a total area of ca. 350,000 km^2 (Fig. 1).

By about 2.5 Ga, the Archean continental crust of the Karelian granite-greenstone terrane underwent tectono-magmatic reactivation during the Karelian stage. This episode of reactivation was initiated by continental rifting, as evidenced by the deposition of conglomerates, quartzites, and arkoses. Subsequently, areally extensive mafic lavas of the Sumi-Sariola Group erupted, followed by the emplacement of mafic-ultramafic layered intrusions and rapid sedimentation in fault-bounded shallow-water basins (Gaál and Gorbatschev, 1987; Gorbatschev and Bogdanova, 1993). Most of the Sumian-Sariolian rocks occur in NW-trending volcano-sedimentary belts, reflecting primary controls on deposition and magmatism by a NNW-NW-trending rift-formed fault system. One of these large belts, the Vetreny Belt, is the subject of this study (Fig. 1). The belt can be traced from Lake Vyg southeastward over a distance of more than 250 km; its width increases from 15 to 85 km to the southeast, where it plunges beneath the Paleozoic cover of the Russian platform and extends further southeast (Kulikov, 1988). The Vetreny Belt shows a clear asymmetric structure. In the northeast, it is separated from the Belomorian Block by the Northern deep fault zone. In the southwest, basal quartzites of the Toksha suite unconformably overlie the TTG-complexes of the Vodla Block and the surrounding greenstone belts.

The early Proterozoic rocks of the Vetreny Belt have been subdivided into six major suites (Fig. 1). The lowermost part of the sequence is represented by the terrigenous (quartzites) Toksha suite, andesites and basalts of the Kirichi suite, and polymict conglomerates and sandstones of the Kalgachi suite. They are overlain by terrigenous sediments and basalts of the Kozhozero suite, and, higher in the succession, by the tuffaceous and terrigenous Vilenga suite and the Vetreny suite, which is composed entirely of komatiitic basalts. The total thickness of the early Proterozoic sequences in this area varies between 4 and 8 km (Kulikov, 1983; Sokolov, 1987).

For major, trace element, and Sm-Nd and Pb-Pb isotope studies, thirty-five samples were collected from the lowermost Kirichi suite and the uppermost Vetreny suite at five localities, covering the whole territory of the belt. Large representative sample sets were obtained for the Golets Hills area, where three different lava flows were sampled, and for a lava lake (see below) in the Lion Hills area. In order to estimate the time of emplacement of the volcanic sequences and the duration of the magmatic activity, separates of igneous minerals were obtained from Golets Hills lava flow 1, samples from the lava lake, and the Vinela Dike. In the Kirichi area, zircons were obtained from a dacite sample #9307. From the other localities, only few samples were collected in order to complete the general isotope-geochemical picture of the Vetreny Belt (Fig. 1). Given below are brief descriptions of the study areas. In the localities 1–6, the metamorphic grade generally does not exceed the prehnite-pumpellyite facies in places of sample collection, while the rocks from the location 7 are metamorphosed under greenschist facies conditions.

1. The Golets Hills area is located on the northwestern margin of the Vetreny Belt (Fig. 1). Here, four units are recognized (from base upwards): (1) tuffs and tuff-conglomerates with rhythmically banded textures more than 100 m thick; (2) komatiitic basalts (ten flows) with pillow and amygdaloidal textures. The flows vary in thickness between 1.5 and 10 m, and the total thickness of the unit is 90 m; (3) differentiated komatiitic basalt lava flows 20–45 m thick, with a total thickness of 270 m; and (4) komatiitic basalts with pillow and amygdaloidal textures, and rare differentiated flows. The flows are 1.5–5 m thick, and the total thickness of the unit is more than 50 m. Three differentiated

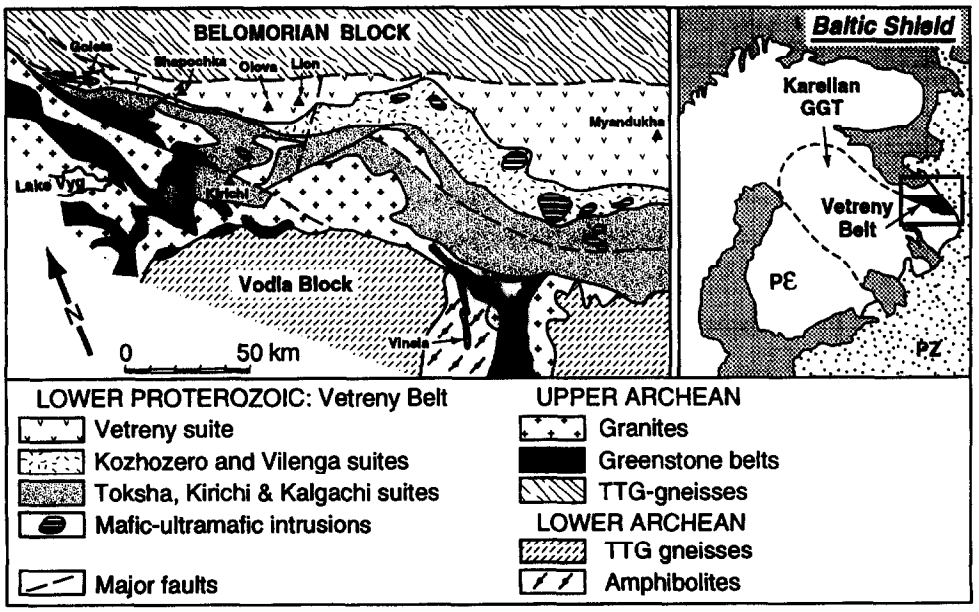

Fig. 1. Geological sketch map of the Vetreny Belt in the Baltic Shield (modified after Kulikov, 1988).

flows of the third member, one from the lowermost part (flow 1) and the other two from the uppermost part of the member, were studied in detail. The flows are similar in structure; each contains flowtop breccia, upper chilled margin, and spinifex and cumulate zones. Detailed petrographic descriptions of the different rock varieties were published elsewhere (Puchtel et al., 1991).

2. The Shapochka-Hills area is located some 40 km to the southeast of Golets Hills. Several dozen massive and pillow lava flows were documented here, ranging in thickness from 10 to 120 m. In the northeastern part of the Vetreny Belt, close to the Northern deep fault zone, the flows show a steep (70–80°) dip to the SW. The rocks are characterized by strong foliation and are metamorphosed under greenschist facies conditions. Towards the SW, the degree of alteration decreases, and the flows are gently (20°) plunging to the NE. In the best exposed interfluve area of the Vetreny Belt range, where one sample was collected from a massive lava flow, the rocks are metamorphosed under the prehnite-pumpellyite facies.

3. In Lion Hills, lava flows are dipping to the NNE at angles of 20–40° and range in thickness from several meters to several tens of meters. The rocks are well exposed and are characterized by the superb state of preservation of primary minerals. The northern slope of the hill is made up of massive and pillow komatiitic basalts. On the southern side, a thick differentiated lava unit is exposed in addition to regular lava flows of the northern-side type. This unit was interpreted as a remnant of a lava lake on the basis of asymmetric structure, the presence of upper breccia, or scoria, and owing to its large thickness and high-Mg composition (Puchtel et al., 1996b). It was named Victoria's Lava Lake after one of its discoverers and was included into the present study.

4. The Olova-Hills area is located some 12 km to the NW of Lion Hills and is characterized by a similar geological structure. The sequence is gently (15°) plunging to the NE and is composed mainly of massive and pillow lava flows. Two spinifex-textured samples were collected from a weakly differentiated lava flow. It consists of flowtop breccia (0.5 m), upper chilled margin (3 m), and a ~8 m thick olivine spinifex-textured zone.

5. The Myandukha-Hills area is located on the southeastern termination of the Vetreny Belt. It is geologically well-studied due to extensive drilling and exploration of stone quarries. The whole sequence is composed of seven massive, amygdaloidal, and pillow komatiitic basalt lava flows ranging in thickness from 14 to 60 m. They show almost horizontal bedding and are intercalated with rare mafic to intermediate tuff horizons. Three samples were collected at intervals of 15 m from a drill core of the uppermost 50 m thick massive flow constituting the top and northern side of the hill Myandukha.

6. The Vinela Dike is confined to the N-S trending Vinela fault zone. The latter shows a nearly vertical dipping and is 0.5–1 km wide and 40–50 km long. The intrusion was traced along strike over a distance of 25 km in the northeastern part of the Vodla Block up to its tectonic contact with the Vetreny Belt (Fig. 1). The intrusion includes a series of lenticular, up to 500 m thick, differentiated ultramafic bodies. These are mostly composed of peridotites and are serpentinized to various extent. The lowermost parts of the bodies are dunitic in composition. The samples come from five drill holes and represent the whole section of the intrusion from the hanging-wall to foot-wall contacts.

7. In the Kirichi-Hills locality, a series of gently (25–30°) plunging flows of massive, pillow, and variolitic komatiitic basalts and andesites 10–50 m in thickness are exposed. They belong to the upper part of the Kirichi suite. The komatiitic basalt flows are subdivided into flowtop breccia, zone of variolitic lavas, and a massive lower part exhibiting columnar jointing, while dacitic lavas are mostly massive throughout. Two komatiitic basalt samples were collected from the massive zone of a 25 m thick lava flow, and a dacite sample from a thick massive flow.

3. ANALYTICAL PROCEDURES

Mineral fractions were separated at the Institute of Geology in Petrozavodsk. About 150 mg of pure augite and 300–500 mg of pigeonite and olivine separates were then obtained at the Institute of Ore Deposit Geology (IGEM) in Moscow by handpicking the ~99% pure concentrates.

Microprobe studies were carried out at the Mineralogisch-Petrographisches Institut, University of Cologne, using a Cameca Camebax electron microprobe. The operating conditions were 15 kV accelerating voltage, 20 nA beam current, and integration time of 10 s per element.

Chemical studies were undertaken on 150 g aliquots from 1 to 3 kg of sample, reduced with a jaw crusher and ground twice in a corundum mill. Major element abundances were determined by X-ray fluorescence on fused glass pellets using a Philips PW-1404 at the Johannes-Gutenberg-University of Mainz. The trace elements Cr, V, Co, Ni, Zr, Y, Sr, and Ba were analyzed on pressed powder pellets on the same XRF-machine. The trace elements Sc, Hf, Nb, Ta, Rb, Th, U, and Pb were determined on an upgraded PlasmaQuad PQ1 ICP-MS at the University of Kiel following the method outlined by Garbe-Schönberg (1993). Rare earth element (REE) concentrations were determined at IGEM in Moscow by isotope dilution mass-spectrometry using the method described by Thirlwall (1982) and modified by Zhuravlev et al. (1989). Accuracies are estimated as follows: major elements: 2% for elements present in concentrations greater than 0.5%; trace elements: 5% for Zr, Cr, V, Co, and Ni; 10% for Y, Sr, and Ba. The ICP-MS analyses yield accuracies of ~5%. For the ID-MS measurements of REE, repeated analyses of the BCR-1 standard established the accuracy for La to be 2% and for the remaining REE as better than 2%.

Sm-Nd isotope investigations were carried out at the Max-Planck-Institut für Chemie in Mainz following the technique described by Chauvel et al. (1985). Neodymium and samarium were run on a MAT-261 Finnigan mass spectrometer under static mode. The effects of fractionation during Nd runs were eliminated by normalizing to $^{146}Nd/^{144}Nd = 0.7219$. $^{143}Nd/^{144}Nd$ isotope ratio measurements of the La Jolla standard during the period of data collection yielded a value of 0.511831 ± 18 ($2\sigma_{pop.}$; $N = 21$). All neodymium isotope ratios were bias-corrected to the La Jolla standard $^{143}Nd/^{144}Nd = 0.511860$. Regression analyses followed the method of York (1966), and the error on the initial ϵNd value was calculated using the method of Fletcher and Rosman (1982). The initial ϵNd values were calculated based on the present-day parameters of the chondrite uniform reservoir (CHUR) adopted from Jacobsen and Wasserburg (1980, 1984) to be the following: $^{147}Sm/^{144}Nd = 0.1967$, $^{143}Nd/^{144}Nd = 0.512638$. The reported analytical uncertainties used in the regression calculations were 0.2% for $^{147}Sm/^{144}Nd$ and for $^{143}Nd/^{144}Nd$, the $2\sigma_{pop.}$ value for the La Jolla standard corresponding to its external reproducibility.

Lead isotope data were obtained at the Max-Planck Institut für Chemie in Mainz using a MAT-261 Finnigan mass spectrometer and following the methods described by Dupré et al. (1984) and Dupré and Arndt (1990). Small chips of rock (0.5–1 g) were leached in hot 6N HCl for 30–60 min to remove Pb that may have been introduced during sample preparation or secondary processes. Lead was then separated using the method of Manhès et al. (1978).

Table 1. Representative microprobe analyses of olivines

Location	Golets Flow 1			Golets Flow 3		Lion Hills			Vinela Dike		
Sample no.	8991	8991	8991	89100	8952	91112	91112	91106	94175	94175	94175
SiO_2	39.24	39.48	39.8	39.43	39.85	40.28	40.77	40.00	40.47	40.49	40.3
TiO_2	0	0	0.01	0.015	0.024	0	0.03	0	0	0	0
Al_2O_3	0	0.048	0.069	0.074	0.039	0.04	0.012	0.017	0	0	0
Cr_2O_3	0.12	0.081	0.11	0	0.18	0.2	0.14	0.096	0.03	0.04	0.03
FeO	12.83	13.28	13.14	12.05	12.03	10.67	10.91	10.81	10.55	10.45	10.17
MnO	0.17	0.18	0.18	0.19	0.18	0.177	0.13	0.143	0.15	0.18	0.14
NiO	0.37	0.18	0.25	0.25	0.37	0.28	0.31	0.223	0.52	0.51	0.51
MgO	46.76	46.42	45.72	47.42	47.05	48.07	48.06	47.46	48.51	48.15	48.48
CaO	0.28	0.36	0.4	0.26	0.29	0.3	0.37	0.22	0.04	0.06	0.03
Total	99.78	100.05	99.67	99.67	100.00	100.02	100.73	98.98	100.27	99.88	99.66
%Fo	86.66	86.17	86.12	87.52	87.46	88.93	88.70	88.67	89.10	89.20	89.50

The total blank was about 150 pg and is negligible compared to the Pb concentrations in the rocks (1.5–5 ppm). The analyses were corrected for isotopic fractionation, which was determined by analysis of the standard NBS-982 (sixty-seven analyses during the period of data collection) to be 1.0012 ± 0.00049 (2σ) per atomic mass unit. Error input was determined by mass fractionation of approximately 0.04% per mass unit. The μ_1 value was calculated using a single-stage model, assuming 4.50 Ga as the age of the Earth and Canyon Diablo values (Tatsumoto et al., 1973) for the starting isotopic composition. In order to calculate the age, $^{207}Pb/^{204}Pb$ and $^{206}Pb/^{204}Pb$ data were regressed using the York (1969) procedure, the ISOPLOT program (Ludwig, 1992), and assuming an error correlation coefficient of 0.9. All errors on ages and initial isotopic ratios are quoted at 2σ or 95% confidence level.

U-Pb isotope analyses of zircons were performed at the Curtin University of Technology in Perth, Western Australia. Zircon grains selected for the analysis were air-abraded using pyrite as a polishing agent and the technique developed by Krough (1982). After abrasion, zircons were washed in 4N HNO_3 to remove pyrite. Digestion, chemical separation, mass spectrometry, and data reduction followed the procedures described by Nemchin et al. (1994). Total procedural blank for Pb measured for the sample set studied was ~10 pg.

4. RESULTS

4.1. Compositions of Olivines

Olivines from the cumulate zones of the two differentiated Golets lava flows (1 and 3), Victoria's Lava Lake, and from the Vinela Dike dunites range in composition between $Fo_{86.1\text{-}86.7}$, $Fo_{87.4\text{-}87.5}$, $Fo_{88.7\text{-}88.9}$, and $Fo_{89.1\text{-}89.5}$, respectively. Representative data for the most magnesian cores of individual grains are listed in Table 1.

4.2. Chemical Compositions of the Rocks

Major, trace, and rare earth element data for the samples from the study areas normalized to 100% on a volatile-free basis are listed in Table 2 and shown in the variation diagrams (Figs. 2–4).

Puchtel et al. (1996b) have considered the problem of element mobility in Victoria's Lava Lake. Most components were shown to have been immobile during low-grade metamorphism. Some mobility was established for K_2O, Rb, and, to a lesser extent, for Na_2O. Generally, the samples of volcanic rocks from the Vetreny Belt have volatile contents between 0.2 and 5%; in the Vinela Dike rocks the volatile contents increase to 9–16%, reflecting variations in degrees of alteration and/or in modal olivine abundances. Most of the volcanic rocks, especially those from Lion Hills and Golets Hills (flow 3) are characterized by remarkable preservation of igneous phases. In several samples from the lava lake, primary volcanic glass is preserved despite the fact that it is very susceptible to alteration and devitrification. We studied it using both optical methods and an electron microprobe and found several glass-like areas with less than 1% LOI, to which the term glass was applied (Puchtel et al., 1996b). Thorough inspection of the data allowed us to extend the conclusion about the essentially immobile behavior of petrogenetically important components to all the samples analyzed in this study.

MgO contents vary between 7 and 26% in the komatiitic basalt lava flows and increase to 37% in the Vinela Dike peridotites and to 46% in the dunite. MgO contents in flowtop breccias and upper chilled margins of the lava flows 1 and 3 in the Golets Hills area are 12.9 and 13.6%, and those in the upper chill of the lava lake in Lion Hills are 14.7%. The dacite sample #9307 plots well outside the compositional range for the komatiitic basalts. It is considered as being petrogenetically unrelated to the magnesian lavas and was excluded from the follow-up petrogenetic modeling. Most components show strong (r = 0.92–1.0) correlations with MgO contents and vary in a manner (negative relationships for Al, Ti, Ca, V, Zr, Nb, Y, REE, Th, U, and positive for Ni) entirely consistent with olivine fractionation (Fig. 2). When plotted against wt% MgO, the analytical data fall on olivine control lines, which intersect the MgO axes at 46.1, 47.2, and 47.9% for Golets flows 1 and 3 and the lava lake, respectively, and at 48.7% for the Vinela Dike. Chromium is positively correlated with MgO in the lavas and shows a substantial decrease in the Vinela Dike rocks. It suggests that along with olivine, chromite was a liquidus phase over the whole compositional range of the crystallization of the lavas but did not fractionate during the formation of the intrusion.

The variation diagrams (Fig. 2) reveal both similarities and substantial differences in the compositions of the erupted liquids of the Vetreny suite lavas. Interestingly, the largest differences in lava compositions are observed within the Golets Hills area between flow 1 on the one hand and flows 2 and 3 on the other hand. The rocks from the other regions, some up to 250 km away from Golets Hills, have intermediate compositions between these two endmembers. All the lavas follow the same trend in Al_2O_3 vs. MgO diagram (Fig. 2) and show only slight differences in the relative abundances of Y and HREE. The rocks from Golets flows 2 and

Table 2. Major and trace element data

Sample	Golets flow 1						Golets flows 2 and 3						Shapochka and Olova			Kirichi		
	8978	8984	8987	8990	8991	8993	8971	8964	8996	8999	8954	8957	9301	9302	9303	9305	9306	9307
SiO_2	49.6	52.5	52.8	53.5	46.5	48.6	51.0	46.4	49.5	50.5	45.4	47.4	50.8	50.2	50.2	52.0	53.6	63.8
TiO_2	0.70	0.70	0.72	0.79	0.43	0.48	0.81	0.5	0.72	0.76	0.46	0.56	0.63	0.61	0.6	0.68	0.65	0.59
Al_2O_3	12.6	12.9	13.1	13.8	7.60	8.56	12.8	7.92	11.0	12.2	7.19	8.88	11.4	11.0	11.0	12.8	12.4	15.6
Fe_2O_3	12.6	11.6	11.8	11.3	13.4	12.0	12.4	13.0	12.7	12.6	13.4	13.4	11.8	11.9	12.0	11.1	10.8	6.39
MnO	0.16	0.18	0.18	0.18	0.19	0.18	0.18	0.18	0.18	0.18	0.18	0.18	0.18	0.17	0.18	0.18	0.17	0.14
MgO	12.9	10.2	8.86	6.80	24.8	22.1	9.23	23.7	13.6	10.7	25.6	20.7	14.0	15.6	15.4	11.4	10.8	3.29
CaO	9.12	9.40	9.47	10.4	6.25	7.20	11.6	7.48	10.4	10.9	6.83	8.05	9.31	8.54	8.87	10.4	9.93	5.87
Na_2O	1.78	2.00	2.52	2.30	0.47	0.44	1.66	0.53	1.34	1.64	0.67	0.63	1.35	1.16	1.05	0.93	1.05	3.06
K_2O	0.45	0.46	0.52	0.72	0.35	0.36	0.23	0.29	0.37	0.39	0.21	0.18	0.52	0.71	0.62	0.57	0.59	1.15
P_2O_5	0.09	0.09	0.10	0.21	0.07	0.07	0.11	0.07	0.10	0.10	0.07	0.08	0.09	0.10	0.10	0.09	0.06	0.08
LOI	2.26	0.81	0.64	0.65	3.72	5.26	0.39	3.55	2.88	0.27	3.20	3.24	1.77	2.66	2.94	2.9	2.67	1.54
Cr	1095	744	640	283	2102	2716	555	2834	1351	797	2803	1803	1309	1797	1643	927	842	100
V	233	212	216	228	138	155	251	164	236	228	158	177	185	196	196	207	199	96
Co	59	51	47	40	105	92	48	97	64	55	102	88	63	67	62	52	51	23
Ni	278	154	118	57	747	878	129	922	362	182	1029	662	391	522	459	173	165	58
Zr	70	69	70	71	41	43	61	38	55	58	35	42	59	56	57	70	67	127
Hf	1.76		1.83		1.04		1.59		1.33	1.41		0.971	1.58	1.36		1.37		2.66
Nb	2.68		2.62		1.50		2.52		2.13	2.31		1.67	4.07	3.08		3.09		4.44
Ta	0.178		0.172		0.102		0.167		0.141	0.150		0.115	0.136	0.119		0.167		0.421
Sc	38.8		38.2		23.2		45.4		37.3	39.7		27.5	34.4	30.7		38.3		17.5
Y	15.6	15.4	15.9	17.0	9.66	9.63	17.1	10.5	15.1	15.8	9.85	12.8	13.5	13.4	12.9	14.4	13.9	14.8
Sr	166	237	226	192	112	106	175	103	150	157	100	114	160	189	140	201	162	171
Rb	14	11	10	9	13	20	5	7	6	6	6	6	13	14	18	16	17	40
Ba	356	213	282	278	134	93	94	69	133	148	68	71	158	184	138	238	244	309
Pb	4.39		4.55		2.41		1.94		2.38	1.87		1.89	2.74	2.41		3.00		4.57
U	0.531		0.505		0.271		0.201		0.186	0.203		0.155	0.291	0.217		0.572		0.868
Th	2.43		2.44		1.30		1.01		0.854	0.990		0.687	1.41	1.05		2.80		3.682
La	9.62	10.4	10.2	11.0	5.77	6.35	7.88	4.35	6.33	7.01	4.18	5.00	8.68	7.59	7.84	11.4	11.4	15.7
Ce	21.5	22.2	22.6	23.7	12.7	13.9	16.9	9.97	14.6	16.0	9.41	11.4	17.8	17.0	17.0	24.3	24.2	31.6
Nd	11.3	11.4	11.7	12.4	6.61	7.17	10.8	5.91	8.64	9.37	5.58	6.75	9.87	9.37	9.12	12.2	11.9	13.9
Sm	2.49	2.50	2.59	2.74	1.47	1.60	2.69	1.46	2.14	2.29	1.38	1.67	2.27	2.11	2.07	2.63	2.57	2.87
Eu	0.655	0.771	0.769	0.828	0.450	0.498	0.905	0.485	0.706	0.746	0.453	0.549	0.721	0.662	0.625	0.768	0.768	0.838
Gd	2.50	2.52	2.58	2.80	1.49	1.64	3.01	1.63	2.37	2.52	1.52	1.84	2.44	2.19	2.17	2.62	2.54	2.85
Dy	2.50	2.52	2.60	2.83	1.51	1.65	3.24	1.73	2.54	2.67	1.63	1.96	2.59	2.24	2.27	2.61	2.53	2.64
Er	1.49	1.51	1.56	1.68	0.913	1.00	1.95	1.04	1.52	1.61	0.979	1.18	1.62	1.34	1.36	1.53	1.48	1.54
Yb	1.40	1.42	1.47	1.58	0.865	0.950	1.82	0.975	1.40	1.50	0.917	1.11	1.58	1.29	1.29	1.37	1.33	1.48

Note. Analyses are normalized to 100% on an anhydrous basis

Table 2 (continued)

Sample	Lion-Hills (Victoria's Lava Lake)									Myandukha Hills			Vinela Dike				
	91101	91103	91104	91105	91106	91110	91112	91113	91117	94170	94171	94172	8803/1	94173	94174	94175	94176
SiO_2	52.4	48.2	47.9	46.0	47.8	50.3	50.5	49.3	51.3	50.4	49.9	51.0	43.8	44.3	43.8	39.9	45.2
TiO_2	0.67	0.49	0.46	0.38	0.45	0.58	0.59	0.59	0.66	0.63	0.63	0.65	0.34	0.27	0.24	0.06	0.30
Al_2O_3	13.2	9.03	8.81	7.31	8.50	11.1	11.5	11.5	12.9	11.6	11.4	11.8	4.23	4.03	3.14	0.92	3.77
Fe_2O_3	11.1	11.9	11.7	12.3	11.7	12.1	11.6	11.3	11.7	12.2	12.4	12.3	12.1	10.6	12.7	11.6	12.1
MnO	0.19	0.17	0.18	0.18	0.18	0.18	0.17	0.18	0.20	0.18	0.18	0.17	0.18	0.17	0.18	0.18	0.18
MgO	8.85	20.4	21.6	26.1	22.6	14.7	13.7	14.5	10.1	13.4	14.4	13.7	34.8	37.1	36.1	46.5	34.4
CaO	10.7	7.62	7.26	5.88	7.00	8.96	9.59	10.4	10.4	9.85	10.0	8.75	4.22	3.31	3.69	0.60	3.72
Na_2O	2.21	1.89	1.68	1.62	1.28	1.63	2.03	1.90	2.52	1.28	0.76	1.24	0.02	0.03	0.02	0.16	0.03
K_2O	0.47	0.26	0.32	0.22	0.39	0.43	0.35	0.26	0.13	0.32	0.33	0.37	0.29	0.14	0.06	0.04	0.16
P_2O_5	0.09	0.08	0.07	0.06	0.07	0.08	0.09	0.09	0.09	0.08	0.07	0.07	0.10	0.09	0.10	0.02	0.12
LOI	0.19	1.22	0.69	2.04	0.89	2.50	1.50	2.42	0.18	2.15	2.72	2.92	9.28	10.1	9.4	16.2	8.76
Cr	688	2417	2255	3507	2131	1619	1570	1552	898	1331	1373	1354	1179	1206	1689	1262	1662
V	253	176	167	137	161	207	214	219	246	209	206	213	85	76	70	21	91
Co	47	87	91	107	96	67	56	58	53	63	65	63	102	129	137	157	124
Ni	119	801	874	1138	952	408	348	386	174	373	436	395	2327	2588	2651	3254	2456
Zr	63	44	43	34	40	52	54	56	61	52	52	55	28	32	25	5	28
Hf	1.58		1.07		1.01				1.50	1.35		1.23	0.842		0.547		0.707
Nb	2.12		1.37		1.28				2.03	1.88		1.88	1.27		0.890		1.06
Ta	0.137		0.090		0.085				0.134	0.126		0.133	0.104		0.076		0.082
Sc	45.8		25.6		25.8				40.9	34.9		34.2	12.8		10.1		14.8
Y	16.0	11.5	11.0	8.70	10.1	13.5	14.2	14.4	15.5	13.3	13.4	14.4	5.47	5.51	5.47	1.16	6.53
Sr	165	116	115	90	109	154	152	161	158	146	131	129	12	36	9	7	66
Rb	8	5	7	4	9	10	9	5	3	7	8	10	19	7	4	2	8
Ba	197	97	125	95	123	106	242	236	150	91	95	107	55	37	10	3	67
Pb	2.32		1.80		1.43				2.01	1.69		1.45	1.50		1.51		1.54
U	0.254		0.182		0.171				0.254	0.205		0.230	0.258		0.195		0.199
Th	1.19		0.824		0.709				1.18	0.969		0.986	0.972		0.778		0.830
La	7.75	5.54	5.38	4.27	5.05	6.52	6.78	7.60	7.59	6.82	7.09	7.40	4.01	4.54	2.57	0.730	3.58
Ce	17.3	12.3	11.9	9.46	11.2	14.5	15.1	16.6	16.8	14.9	15.7	16.7	8.65	9.30	5.49	1.51	7.47
Nd	9.63	6.91	6.68	5.30	6.34	8.24	8.45	9.09	9.43	8.55	8.72	9.35	4.45	4.24	2.91	0.740	3.93
Sm	2.28	1.65	1.59	1.26	1.50	1.94	2.03	2.10	2.23	2.06	2.09	2.21	1.04	0.921	0.702	0.173	0.932
Eu	0.734	0.528	0.508	0.404	0.494	0.634	0.672	0.646	0.716	0.668	0.674	0.708	0.313	0.280	0.221	0.053	0.286
Gd	2.47	1.75	1.71	1.36	1.61	2.13	2.19	2.21	2.41	2.28	2.26	2.38	1.11	0.936	0.786	0.184	0.989
Dy	2.64	1.88	1.83	1.46	1.73	2.26	2.34	2.33	2.58	2.48	2.44	2.55	1.14	0.898	0.816	0.182	0.985
Er	1.62	1.15	1.12	0.896	1.06	1.37	1.42	1.42	1.58	1.55	1.53	1.60	0.630	0.492	0.467	0.105	0.537
Yb	1.53	1.11	1.08	0.865	1.02	1.32	1.37	1.35	1.51	1.50	1.49	1.55	0.547	0.438	0.416	0.101	0.473

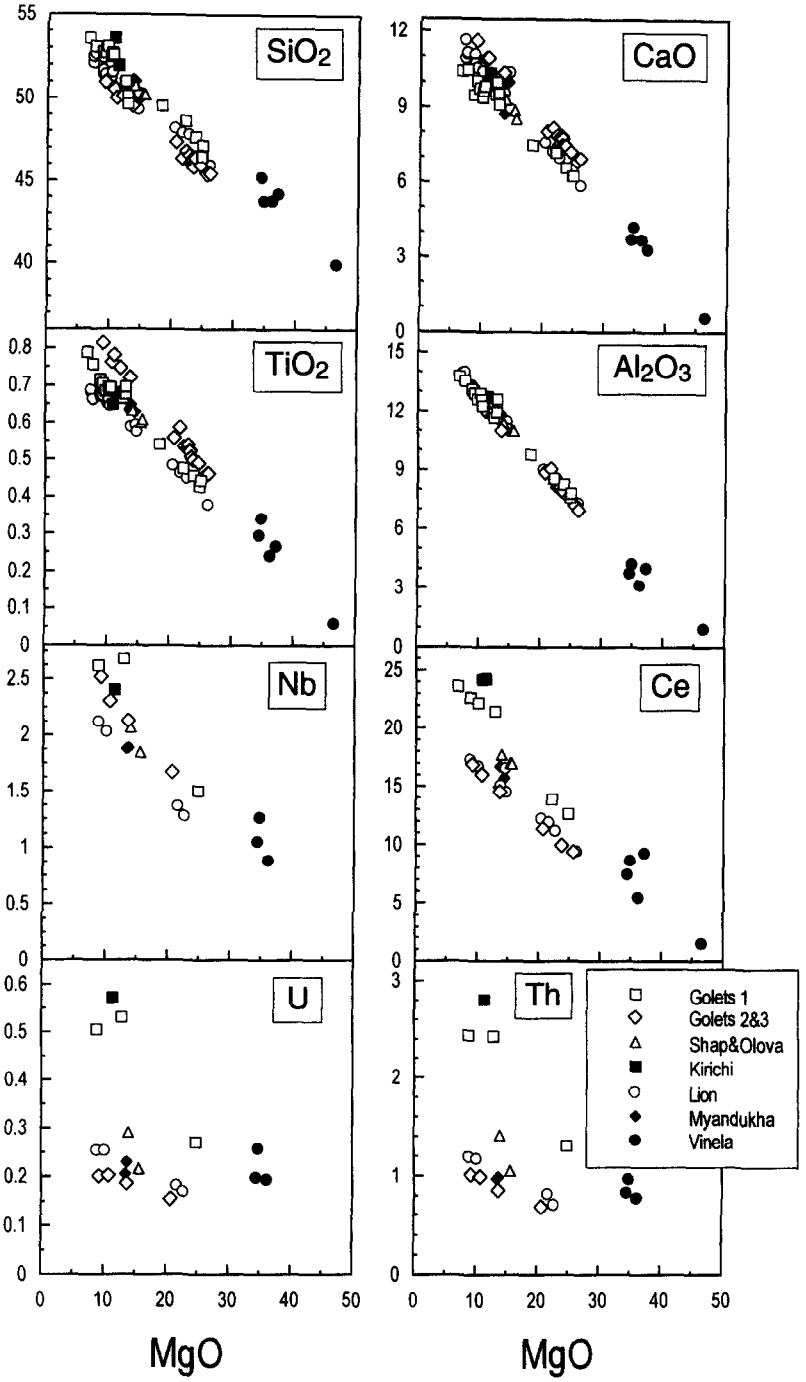

Fig. 2. Variation diagrams of selected major and trace elements for Vetreny Belt rocks.

3 have higher CaO, $Fe_2O_3^t$, TiO_2, V, Y, Nb, and HREE, but lower SiO_2, Zr, U, Th, and LREE contents at given MgO abundances compared to flow 1 and the rocks from the other localities. CaO/Al_2O_3 ratios in flows 2 and 3 are 0.93, similar to the average mantle peridotite and to most other komatiites of late Archean age (Herzberg, 1995), while in flow 1 and the lava lake these are slightly lower (0.77 and 0.82, respectively). Al_2O_3/TiO_2 ratios vary between 18.0 and 19.6 in flow 1 and the lava lake and 15.7 in flows 2 and 3, which is lower than the chondritic value of 22 (Hart and Zindler, 1986; McDonough and Sun, 1995).

As can be seen in the chondrite- and primitive mantle-normalized plots (Figs. 3 and 4), all the rocks are enriched in LREE and other large ion lithophile elements concentrated in the continental crust, especially in Ba, Th, U, Pb, and Sr and show strong negative Nb-, Ta-, and, to a lesser extent, Ti-anomalies. Generally, the patterns of samples from each locality are strongly parallel, with abundances reversely correlated with MgO content. Golets flows 2 and 3 have the lowest $(La/Sm)_N$ ratios of ~1.9, whereas the Kirichi lavas, Golets flow 1 and the Vinela Dike dunite, have the highest $(La/Sm)_N$ of 2.4–3.1 (see Fig. 8).

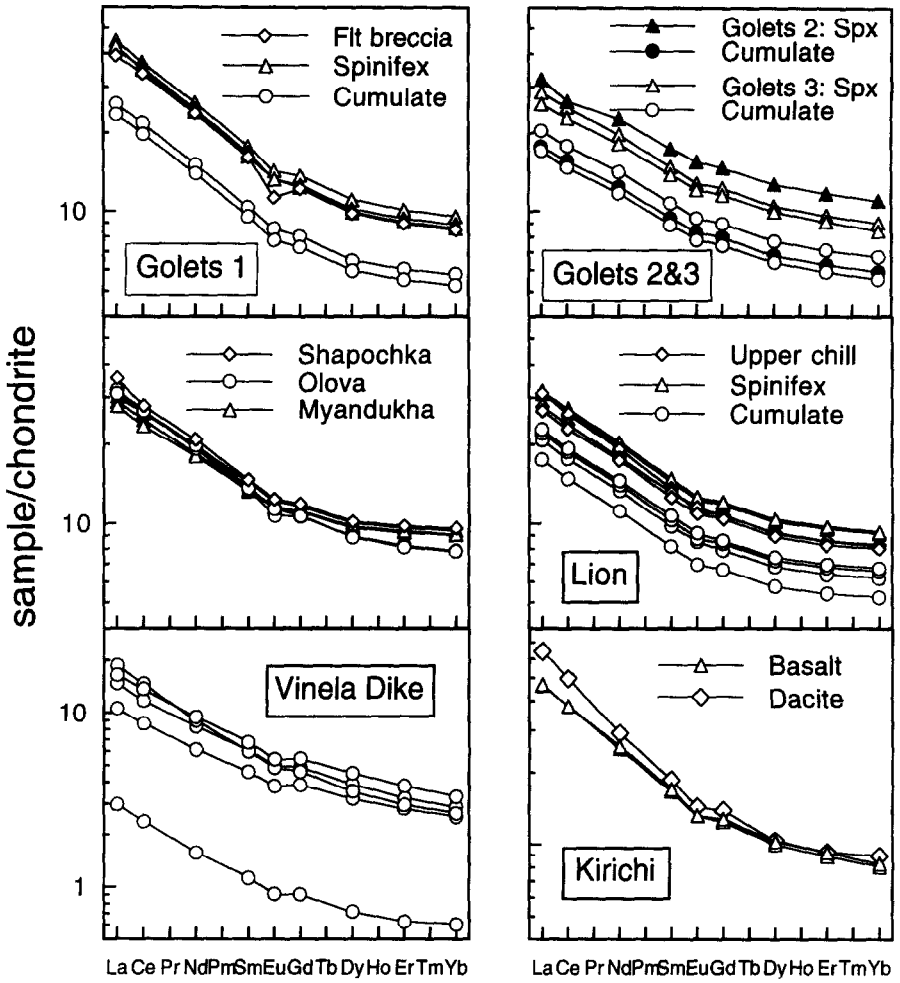

Fig. 3. Chondrite-normalized (Evensen et al., 1978) rare earth element abundances in the Vetreny Belt rocks.

4.3. Sm-Nd Isotope Data

The Sm-Nd isotope data are listed in Table 3 and plotted on the Sm-Nd evolution diagrams (Fig. 5).

4.3.1. Golets Hills

The analytical data for the whole rock samples from flow 1 and for pyroxene-, olivine-, and plagioclase-mineral separates define a reasonably good regression line (MSWD = 1.6) with a slope corresponding to an age of 2449 ± 35 Ma and a negative $\epsilon Nd(T)$ of −1.2 ± 0.3.

4.3.2. Lion Hills

Bulk samples representing the whole 110 m section of the lava lake from top to bottom as well as olivine-, pigeonite-, and augite separates were analyzed. The data define a well-constrained isochron (MSWD = 1.1) with an age of 2410 ± 34 Ma and an $\epsilon Nd(T)$ of −0.9 ± 0.2.

4.3.3. Vinela Dike

In contrast to the two layered lava units described above, the whole rock samples from the Vinela intrusion show substantial differences in Sm/Nd ratios and neodymium isotope compositions. Strictly speaking, the analytical data for bulk samples and olivine and pyroxene separates are not approximated by a single line but define a series of roughly parallel two-points isochrons with ages ranging between 2.24 and 2.57 Ga, with the mean value of 2.41 Ga. Regression of the data for bulk samples 8803/1 and 94175, which have similar isotope compositions, and respective pyroxene and olivine separates gives an age of 2392 ± 26 Ma, $\epsilon Nd(T)$ = −1.6 ± 0.1 (MSWD = 0.2). All analytical data for the intrusion yield a poorly constrained regression line (MSWD = 13) with an age of 2430 ± 174 Ma, $\epsilon Nd(T)$ = −1.4 ± 1.0.

Neodymium isotope compositions of all whole-rock samples from the Vetreny Belt (thirty samples) vary in a wide range and in the conventional Sm-Nd diagram (Fig. 5) define a linear trend with an apparent age of 3027 ± 84 Ma ($\epsilon Nd(T)$ = +3.6 ± 0.6, MSWD = 3.8).

As far as the average isochron age of the samples from different areas is 2430 Ma, we have recalculated ϵNd values for this age. Samples from Golets flows 2 and 3 exhibit the most radiogenic neodymium isotope compositions and have $\epsilon Nd(2430)$ values ranging between 0 and +0.6. Samples from Kirichi Hills and Golets flow 1 with $\epsilon Nd(2430)$ values of −1.4 to −1.8 are among the least radiogenic endmembers. Samples from the Vinela Dike largely overlap the whole

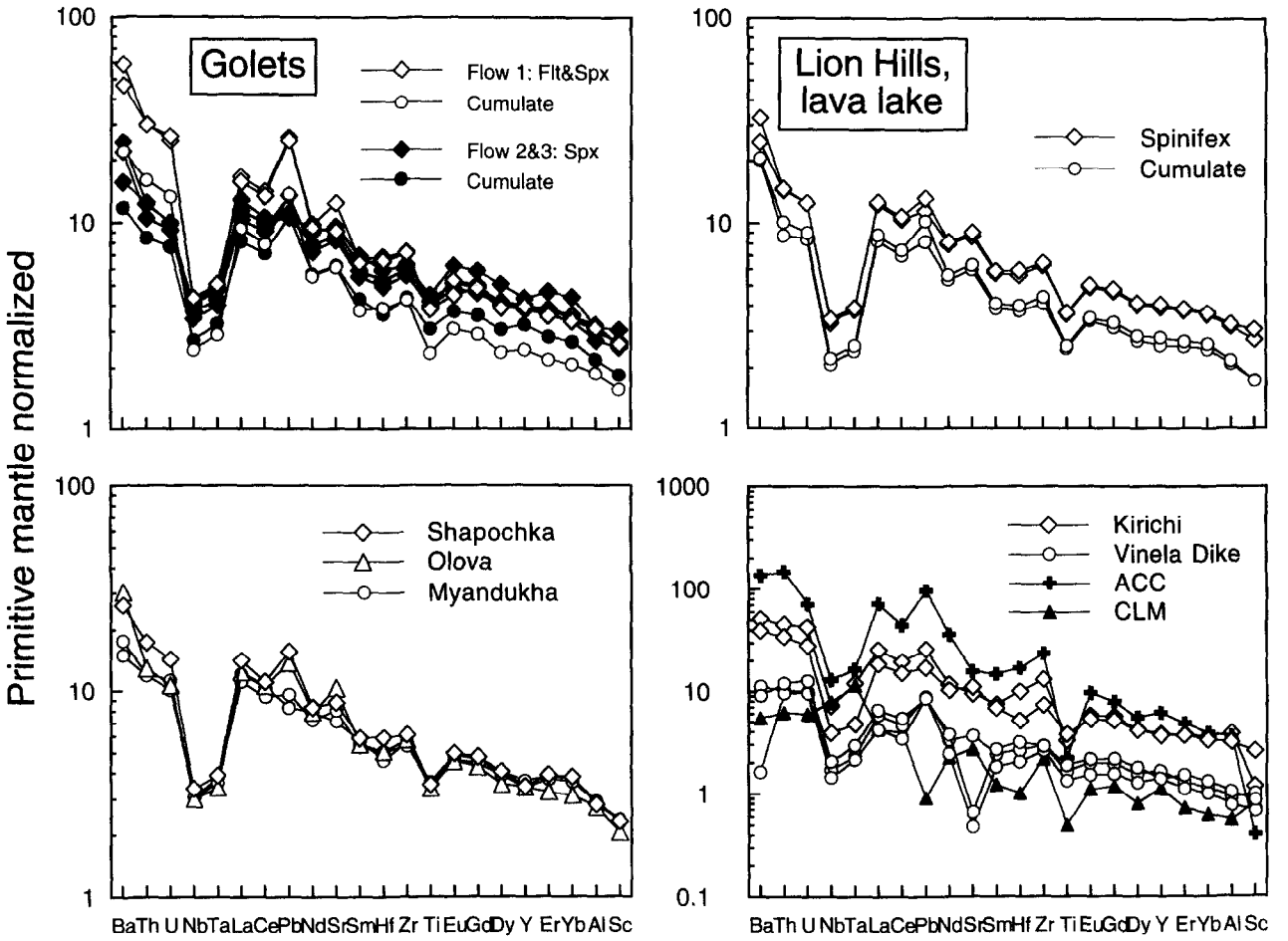

Fig. 4. Abundances of selected major-, trace-, and rare earth elements normalized to primitive mantle values of Hofmann (1988) in the Vetreny Belt rocks.

range of isotope variations in the volcanic rocks [ϵNd(2430) = −0.9 to −1.8 compared with +0.6 to −1.8 in the volcanic rocks].

As can be seen in Table 3, the olivine, pyroxene, and plagioclase separates are characterized by relatively high Nd and Sm concentrations, which are probably due to the presence of tiny glass inclusions in the mineral separates. Calculations show that some 1–10% of these inclusions could account for all the excess Nd. Although these inclusions cannot shift the isotope equilibrium between the crystals and the liquid, and, therefore, do not alter the interpretation of the isochrons, they obviously have substantial effect on the Sm/Nd ratio in the mineral separates. For instance, in Victoria's Lava Lake the measured $^{147}Sm/^{144}Nd$ ratios in the olivines are two and a half times, in the pigeonite almost two times, and in the augites 7–30% lower than the theoretical values calculated on the basis of published distribution coefficients (Green, 1994).

4.4. Pb-Pb Isotope Data

The lead isotope data are reported in Table 4 and plotted in Fig. 6. Samples from the Golets flow 1 define an isochron with an age of 2424 ± 178 Ma. The large error on the age is attributed to the narrow range of variations in the lead isotope ratios, i.e., $^{206}Pb/^{204}Pb$ varies between 17.4 and 18.9. The μ_1, or time-integrated $^{238}U/^{204}Pb$ of the metavolcanics is 9.26 ± 0.05. In the $^{208}Pb/^{204}Pb$ vs. $^{206}Pb/^{204}Pb$ plot the analytical data except for two flowtop breccia samples also define a good regression line. These data allow us to estimate the Th/U ratio for the whole rock series based on the following equation:

$$^{232}Th/^{238}U = S(e^{\lambda 238T} - 1)/(e^{\lambda 232T} - 1)$$

where T (age of the series) is obtained from the $^{207}Pb/^{204}Pb$ vs. $^{206}Pb/^{204}Pb$ diagram, S is the slope of the regression line in the $^{208}Pb/^{204}Pb$ vs. $^{206}Pb/^{204}Pb$ diagram, $\lambda 238 = 0.155125 \times 10^{-9}\ y^{-1}$, and $\lambda 232 = 0.049475 \times 10^{-9}\ y^{-1}$. The calculated Th/U ratio is 4.9 ± 0.3.

4.5. U-Pb Zircon Studies

Zircon grains from the sample #9307 are light brown with length to width ratio of about 2 to 3. On the basis of fine oscillatory zoning, which is identified in transmitted light, zircons are considered to crystallize from the dacite melt rather than represent inherited grains.

Five U-Pb analyses presented in Table 5 and indicated in Fig. 7 show low U concentration and relatively high content of common Pb. However, three grains analyzed have concor-

Table 3. Nd-isotope data

Sample	Sm, ppm	Nd, ppm	$^{147}Sm/^{144}Nd$	$^{143}Nd/^{144}Nd$	εNd(2430)
			Golets Flow 1		
8993 WR	1.517	6.816	0.13455	0.511559 ± 8	-1.64
8993 Cpx	0.9960	2.854	0.21086	0.512824 ± 10	
8991 WR	1.407	6.356	0.13384	0.511561 ± 7	-1.37
8991 Cpx	1.120	3.304	0.20490	0.512691 ± 7	
8991 Ol	0.0635	0.3853	0.09959	0.511014 ± 8	
8987 WR	2.557	11.67	0.13249	0.511536 ± 7	-1.44
8987 Pl	0.1818	0.8427	0.13039	0.511516 ± 13	
8978 WR	2.701	12.51	0.13054	0.511506 ± 3	-1.42
8984 WR	2.509	11.56	0.13116	0.511516 ± 4	-1.42
			Golets Flows 2 and 3		
8964 WR	1.409	5.729	0.14882	0.511895 ± 11	0.47
8971 WR	2.654	10.83	0.14812	0.511861 ± 9	0.02
8999 WR	2.270	9.314	0.14735	0.511849 ± 6	0.03
8996 WR	2.094	8.575	0.14764	0.511880 ± 7	0.55
8957 WR	1.636	6.650	0.14874	0.511886 ± 7	0.32
			Lion, Victoria's Lava Lake		
91103 WR	1.631	6.923	0.14238	0.511739 ± 8	-0.57
91103 Augite	1.325	3.724	0.21508	0.512884 ± 8	
91103 Ol	0.1738	0.6245	0.16819	0.512156 ± 9	
91104 WR	1.603	6.808	0.14233	0.511710 ± 7	-1.12
91104 Augite	1.397	3.976	0.21238	0.512826 ± 7	
91104 Pigeonite	0.5630	1.917	0.17751	0.512284 ± 9	
91106 WR	1.522	6.381	0.14420	0.511751 ± 7	-0.90
91106 Augite	1.265	3.699	0.20681	0.512753 ± 8	
91106 Ol	0.0492	0.1681	0.17708	0.512291 ± 11	
91101 WR	2.306	9.731	0.14322	0.511737 ± 7	-0.87
91105 WR	1.2475	5.209	0.14475	0.511764 ± 4	-0.82
91117 WR	2.255	9.516	0.14324	0.511743 ± 8	-0.76
			Shapochka		
9301 WR	2.178	9.624	0.13681	0.511623 ± 7	-1.09
			Olova-Hills		
9302 WR	2.070	9.209	0.13591	0.511642 ± 4	-0.44
9303 WR	2.004	8.870	0.13660	0.511636 ± 9	-0.77
			Myandukha		
94170 WR	1.994	8.390	0.14370	0.511750 ± 6	-0.77
94171 WR	2.029	8.557	0.14332	0.511756 ± 5	-0.53
94172 WR	2.168	9.171	0.14294	0.511740 ± 4	-0.72
			Kirichi		
9305 WR	2.605	12.12	0.12995	0.511485 ± 7	-1.64
9306 WR	2.541	11.84	0.12972	0.511474 ± 6	-1.79
9307 WR	2.824	13.68	0.12473	0.511405 ± 6	-1.57
			Vinela Dike		
8803/1 WR	0.8950	3.797	0.14244	0.511696 ± 10	-1.43
8803/1 Cpx	2.339	7.613	0.18574	0.512384 ± 9	
94173 WR	0.7956	3.704	0.12984	0.511473 ± 7	-1.84
94173 Cpx	1.967	7.369	0.16137	0.511939 ± 5	
94174 WR	0.6236	2.581	0.14603	0.511780 ± 7	-0.91
94174 Cpx	2.099	7.302	0.17378	0.512250 ± 5	
94175 WR	0.1528	0.6570	0.14059	0.511674 ± 11	-1.28
94175 Ol	0.0480	0.1546	0.18777	0.512424 ± 17	
94176 WR	0.8123	3.437	0.14283	0.511728 ± 5	-0.92

dant U-Pb systems, and the other two are only about 2% discordant. Five data points define the regression line with MSWD = 0.8 and the upper intercept of 2437 ± 3 Ma. The lower intercept within error is indistinguishable from zero. Weighted mean calculation for the three concordant points gives an age of 2437 ± 4 Ma with MSWD = 0.5.

5. DISCUSSION

5.1. Compositions, Liquidus Temperatures, and Differentiation of the Erupted Magmas

Petrographic observations of the Golets and Lion Hills lavas by Puchtel et al. (1991, 1996b) established that the only minerals present as phenocrysts or cumulus phases are olivine and chromite. It is suggested, therefore, that the evolution of the magmas after eruption was controlled by fractionation of these mineral phases only. This conclusion is supported by the variation diagrams (Fig. 2), in which all elements follow olivine control lines.

In order to deduce the compositions of erupted magmas in different parts of the Vetreny Belt, several independent approaches were used. First, the flowtop breccias/scorias and chilled samples are essentially glassy rocks consisting of phenocrysts in a quenched groundmass. They probably did not experience any post-eruption differentiation and are interpreted to have bulk compositions similar to that of the liquids from which they have formed. Secondly, most of lava units contain fresh olivine (Table 1). These data can

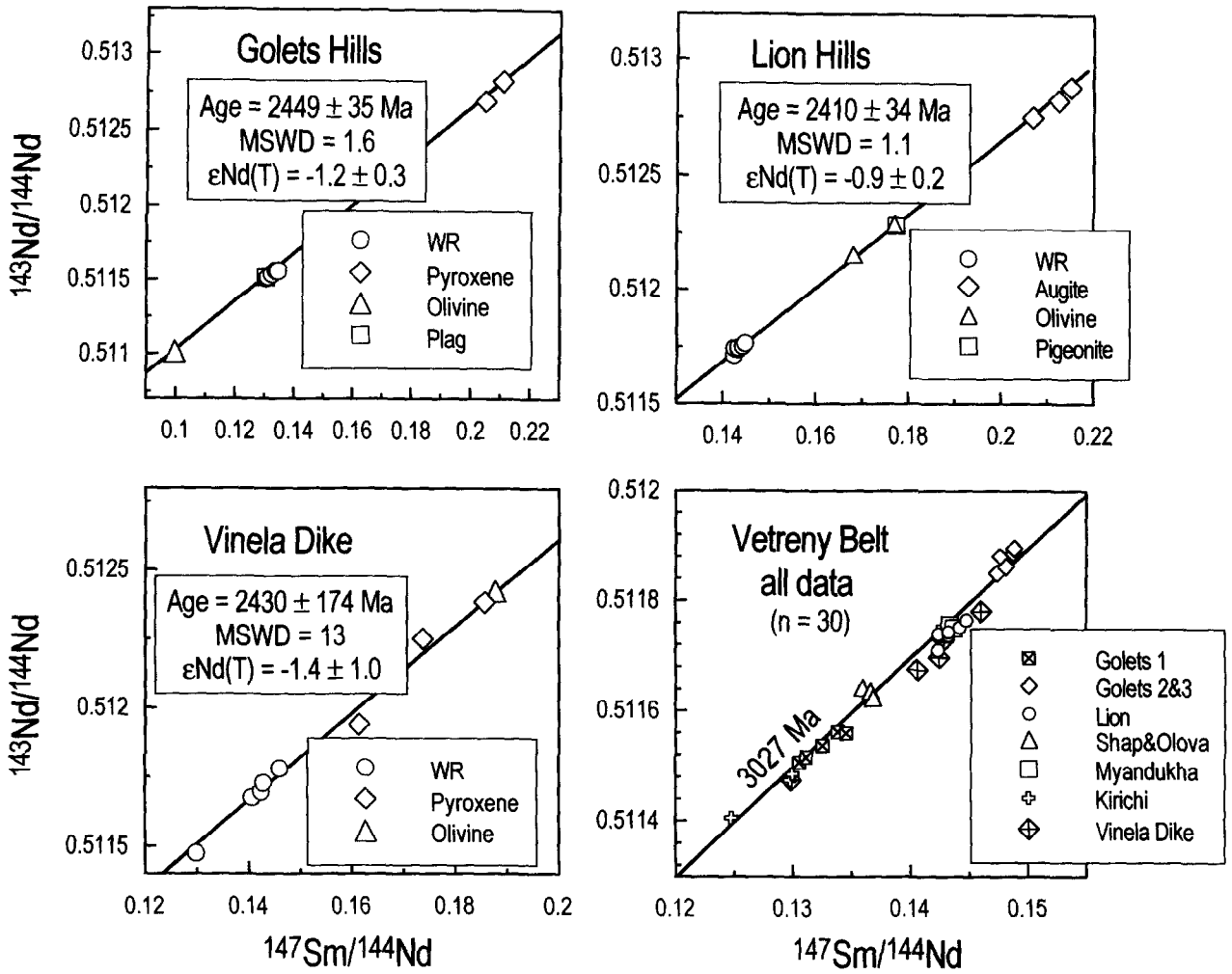

Fig. 5. Conventional Sm-Nd diagrams for whole rock samples and mineral separates from the Vetreny Belt.

be used to infer the composition of the melt from which the olivines have crystallized applying the experimentally determined Fe/Mg distribution coefficients of Beattie et al. (1991) and Roeder and Emslie (1970). In the third approach, the olivine control lines for the elements that are excluded from the olivine crystal lattice can be traced to their intercept with the MgO axis (Fig. 2). These intercepts define the average composition of the liquidus olivine. The results of these estimates for different components are summarized in Table 6 and are in good agreement within each dataset. The calculated MgO contents of the erupted liquids vary between 12.8% and 13.9% in Golets and Myandukha Hills (northwestern and southeastern terminations of the belt) and 15.0 and 15.5% in Lion and Olova Hills in the central Vetreny Belt. It is also possible to estimate the composition of the liquid parental to the Vinela Dike due to the fact that the dunite sample 94175 consists almost entirely of olivine, and its analytical point on the variation diagrams (Fig. 2) plots very close to the MgO-axis, while the peridotites contain variable proportions of pyroxene and plot well above the MgO axis. Regression of the analytical data for the Vinela Dike samples gives an average of 48.7% MgO in the fractionating olivine ($Fo_{89.9}$), in agreement with the microprobe data on the olivines from the dunite sample ($Fo_{89.5}$, Table 1). Olivine of this composition can be shown to be in equilibrium with a liquid containing ~17.3% MgO (Table 6). Thus, the MgO contents of the erupted magmas appear to increase from 13% on the margins to 17% towards the center of the Vetreny Belt.

In order to calculate liquidus temperatures of the erupted melts, the methods of Nisbet et al. (1993) and Abbott et al. (1994) were adopted. The chemical analyses of the chilled samples from different localities were used to calculate the eruption temperatures on the basis of the relationship between the Fe/Mg ratio in a primitive magma and its liquidus temperature (Hanson and Langmuir, 1978; Roeder and Emslie, 1970). The obtained liquidus temperatures show an increase from 1370 to 1440°C towards the center of the belt (Table 6) and correspond to the mantle potential temperatures range of 1530–1630°C.

The increase in eruption temperatures towards the center of the belt may indicate either a thinner lithosphere (i.e., slower temperature drop during ascent) or a higher mantle temperature beneath the central part of the belt. Assuming a temperature drop of ~0.6°C km^{-1} during ascent (McKenzie and Bickle, 1988), a ~70°C higher temperature in the center would suggest an about 100 km thinner lithosphere. This estimate seems unreasonable, as there is no negative

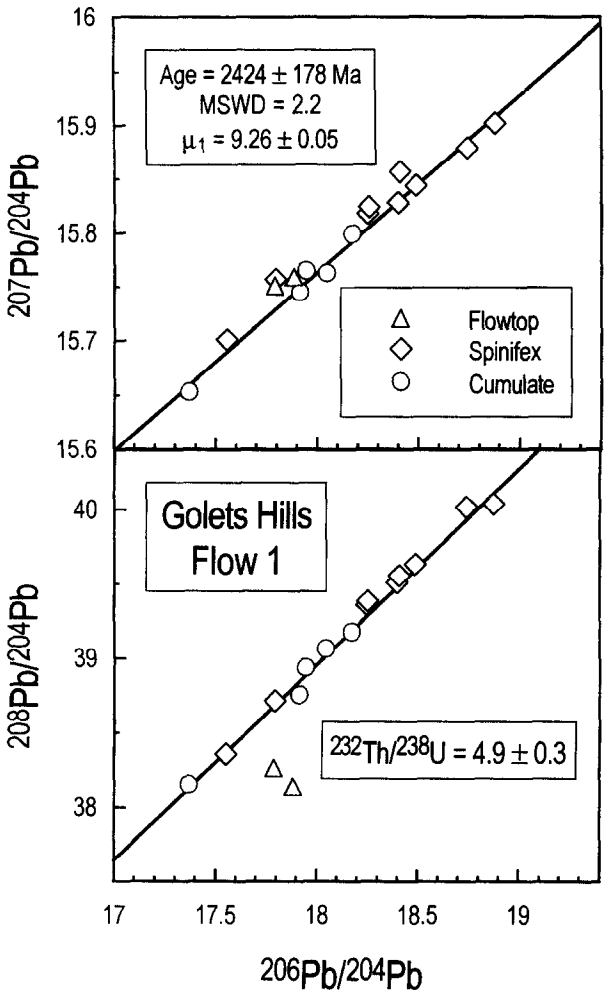

Fig. 6. Pb-Pb evolution diagrams for Golets flow 1 whole rock samples.

correlation between the eruption temperature and degree of contamination (see section below), which would be expected for magmas passing through the continental lithosphere of variable thickness. We suggest, therefore, that the mantle temperatures in the center of the Vetreny Belt were higher than at its margins. A temperature gradient of ~100°C over a region of 300 km in diameter may be expected to be found between the axis and the edge of a plume head (McKenzie and Bickle, 1988; Watson and McKenzie, 1991). The elevated (1440°C) liquidus temperatures of the komatiite magmas imply that the source of the Vetreny Belt komatiites had a substantially higher (1630°C) potential temperature than the ambient mantle temperature of ~1480°C at 2.4 Ga (Richter, 1988; Herzberg, 1995). Together with the inferred steep thermal gradient in the Vetreny Belt, this suggests the existence of a mantle plume underlying the region at 2.4 Ga.

5.2. Constraints on the Compositions of the Mantle Sources

Despite the large compositional differences between the continental crust and the upper mantle, the occurrence and extent of crustal contamination in komatiite and basalt magmas cannot be easily constrained. This is ascribed to the fact that, in some instances, the influence of crustal contamination is almost indistinguishable from the geochemical effects on the magmas derived from a depleted asthenospheric source and then mixed up with a component of the ancient continental lithosphere (Brandon et al., 1993; Glazner and Farmer, 1992). Several authors suggested that primitive magmas erupting in continental rift settings are derived from enriched sources residing in the continental lithospheric mantle (e.g., Hawkesworth et al., 1984, 1988). Ryabchikov et al. (1988) proposed that the Vetreny Belt lavas were derived from the enriched continental lithospheric mantle because of their apparent large scale homogeneity. This in turn implies a common uniform source for these lavas. However, our more complete dataset indicates that the studied rocks from different localities have variable trace element and isotope characteristics. These variations can be ascribed either to the differences in compositions of their mantle sources and conditions of partial melting, to variable contributions from the continental crust, or to the combined effects of both these factors.

Due to very high liquidus temperatures, low viscosities and low incompatible element concentrations komatiitic melts are very susceptible to contamination by upper crustal rocks (Arndt, 1986; Arndt and Jenner, 1986). In many cases contamination occurs during ascent or eruption (Huppert et al., 1984; Huppert and Sparks, 1985) and results in a sharp increase in the abundances of SiO_2, Ba, Th, U, and LREE in asthenospheric melts, but will have little effect on Ta, Nb, HREE, and Ti concentrations. On average, this causes the origin of negative Ta-, Nb-, and Ti-anomalies in crustally contaminated rocks. In contrast, the average subcontinental lithospheric mantle is enriched in Nb and Ta relative to Th and La (Fig. 4; McDonough, 1990). Consequently, mixing with the material of the subcontinental lithospheric mantle will not produce such kinds of anomalies in asthenosphere-derived melts. The Vetreny Belt komatiitic rocks exhibit strong negative Nb- and Ta-anomalies relative to neighboring elements with a comparable degree of incompatibility, i.e., La and Th [$(Nb/La)_N$ = 0.40–0.25, $(Nb/Th)_N$ = 0.11–0.33, Fig. 4]. The rocks with the lowest Nb/Th and

Table 4. Pb isotope data for Golets Hills flow 1

Samples	$^{206}Pb/^{204}Pb$	$^{207}Pb/^{204}Pb$	$^{208}Pb/^{204}Pb$	μ_1**
8978	17.789	15.751	38.263	9.29
8978*	17.882	15.759	38.137	9.28
8982	18.876	15.902	40.038	9.25
8984	18.247	15.818	39.362	9.28
8984*	18.253	15.824	39.387	9.29
8986	18.407	15.857	39.557	9.31
8987	17.794	15.757	38.714	9.30
8987*	17.552	15.701	38.358	9.26
8989	18.398	15.828	39.510	9.25
8990	18.740	15.879	40.015	9.24
8990*	18.487	15.844	39.632	9.25
8991	18.045	15.763	39.065	9.23
8991*	17.944	15.765	38.937	9.27
8993	18.172	15.799	39.178	9.26
8994	17.367	15.653	38.154	9.22
8995	17.913	15.745	38.754	9.23

*Separate chips from the same sample
**Calculated assuming a 4.50 Ga as the age of the Earth

Table. 5. U-Pb zircon data for dacite sample #9307

Grain#	Sample weight (μg)	U (ppm)	Pb (ppm)	$^{206}Pb/^{204}Pb$	$^{206}Pb/^{238}U$	$^{207}Pb/^{235}U$	$^{207}Pb/^{206}Pb$	$^{207}Pb/^{206}Pb$ age	Disc(%)
1	15	72	40	686	0.4590±24	10.02±6	0.1584±4	2439±4	0.15
2	15	26	15	245	0.4602±52	10.02±9	0.1579±10	2433±10	-0.34
3	11	88	46	545	0.4459±18	9.70±5	0.1578±5	2432±6	2.4
4	12	40	21	827	0.4592±36	10.00±8	0.1580±5	2434±5	-0.1
5	19	57	29	1890	0.4478±22	9.75±5	0.1580±4	2433±3	2.1

Nb/La ratios also have the highest SiO_2 abundances at a given MgO content. We argue on this basis that the evolution of the magmas parental to the lavas and the intrusion was mainly controlled by contamination with felsic crustal rocks.

As can be seen in Fig. 8, a positive correlation exists in the diagrams $(Nb/Th)_N$ vs. ϵNd and a negative one in the diagrams $(La/Sm)_N$ vs. ϵNd, $(La/Sm)_N$ vs. $(Nb/Th)_N$, and $(Nb/Th)_N$ vs. Zr/Y. These trends can all be explained by mixing of a magma from a relatively depleted mantle source with high $\epsilon Nd(T)$, Nb/Th, Nb/La, but low Zr/Y and La/Sm ratios with an enriched component like the Archean continental crust having low $\epsilon Nd(2430)$, Nb/Th, Nb/La, and high Zr/Y and La/Sm values. On the other hand, these chemical parameters do not change within the single lava units, though they are quite variable in different lenticular bodies of the Vinela Dike (Fig. 8). This implies that contamination of the lavas occurred mainly en route to the surface and not after the eruption. The lenticular bodies of the Vinela Dike probably represent intrusions derived from a common magma which were contaminated to different extent by wall rocks. This may have occurred in intermediate magma chambers during the periodical replenishment of the dike.

The positive correlation between Eu/Eu* and ϵNd (Fig. 9) suggests that the negative Eu-anomalies in the studied rocks resulted from crustal contamination. Assuming that the Eu/Eu* in uncontaminated rocks must be close to 1, we tried to estimate the $\epsilon Nd(2430)$ value in the primary melt and, consequently, in the magma source region. First, we removed several samples in which Eu-anomalies were interpreted to be the result of secondary alteration processes. These include the Vinela Dike samples with high (up to 16%) LOI and samples from the flowtop breccias, where trivalent Eu is reduced to Eu^{2+} under high-temperature conditions and is then easily leached during seawater interaction

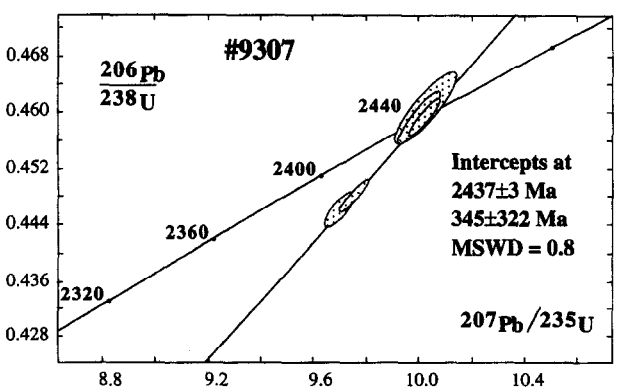

Fig. 7. U-Pb concordia diagram for zircons from dacite sample #9307.

(Michard and Albaréde, 1986; Bau, 1991). We have also screened out several samples with abundant amygdules. Regression calculations for the least altered samples indicate an $\epsilon Nd(2430)$ value in the primary magma of approximately +2.6 (Fig. 9). Using this ϵNd value we then calculated the incompatible element ratios from respective correlations. These calculations show that the primary melt was moderately depleted in highly incompatible elements and had $(La/Sm)_N$ of 0.9, $(Zr/Y)_N$ of 0.9, and $(Nb/Th)_N$ of 0.6.

Available data suggest the existence of around 50 km thick continental crust in the Karelian granite-greenstone terrane, seismically grouped into 20–30 km of lower crust, 7–17 km of middle crust, and 10 km of upper crust (Luosto et al., 1989). The upper crust in the adjacent Vodla and Belomorian Blocks consists of TTG-gneisses metamorphosed under amphibolite to granulite facies conditions with ages of 3.1–3.2 and 2.6–2.8 Ga, respectively (Kulikov et al., 1990; Bogdanova and Bibikova, 1993; Lobach-Zhuchenko et al., 1993; Timmerman and Daly, 1995; Bibikova et al., 1996). Trace element data for these rocks are not available and in order to estimate the extent of contamination of the primary magmas to the Vetreny Belt rocks, we used a trace-element composition of the average felsic Archaean granulite reported by Rudnick and Fountain (1995). This composition provides the closest approximation to the average composition of the upper crustal rocks in the Vodla and Belomorian Blocks reported by Kulikov et al. (1990) and Lobach-Zhuchenko et al. (1993) in terms of major elements, and thus we assume that it is also a suitable crustal endmember for our mixing model. The average neodymium isotopic parameters for these rocks ($^{143}Nd/^{144}Nd$ = 0.510927, $^{147}Sm/^{144}Nd$ = 0.1011, N = 47) were compiled from the data of Kulikov et al. (1990), Lobach-Zhuchenko et al. (1993), Timmerman and Daly (1995), and Bibikova et al. (1996). As a possible equivalent of the primitive melt giving rise to the Vetreny Belt lavas, we have chosen the composition of a low-magnesian (17.6% MgO) komatiite sample Z2 from the 2.7 Ga Belingwe greenstone belt (Chauvel et al., 1993; Jochum et al., 1991; Nisbet et al., 1987). This komatiite has $^{143}Nd/^{144}Nd$ = 0.513197, $^{147}Sm/^{144}Nd$ = 0.2212, $(La/Sm)_N$ = 0.8, $\epsilon Nd(2.7\ Ga)$ = +2.5, close to the inferred composition of the primary magma for the Vetreny Belt rocks. The results of our calculations are shown in Fig. 10. We used the ratios of selected elements, which are insensitive to olivine + spinel fractional crystallization but are crucial indicators of assimilation processes. Neodymium isotope compositions of the endmembers and the Vetreny Belt rocks were recalculated for the time of the mixing event (2430 Ma). The obtained data support the model that the Vetreny Belt komatiitic basalts were formed by mixing of a komatiite magma depleted in incompatible elements with upper crustal felsic

Table 6. Results of calculations of erupted melt compositions, liquidus and potential mantle temperatures

Sample series	Chill and/or spinifex-zone	Olivine (microprobe data)	Olivine (OCL-intersect)	Average Liq composition	T_{liq}(°C)	T_{pot} (°C)
Golets Hills, Flow 1	12.9% MgO	$Fo_{86.7}$ (46.8% MgO) Equil Liquid: 12.8% MgO	46.1% MgO ($Fo_{86.3}$) Equil Liquid: 12.6% MgO	12.8% MgO	1370	1530
Golets Hills, Flow 3	13.6% MgO	$Fo_{87.5}$ (47.1% MgO) Equil Liquid: 13.9% MgO	47.2% MgO ($Fo_{87.7}$) Equil Liquid: 14.3% MgO	13.9% MgO	1380	1540
Lion Hills, Lava Lake	14.7% MgO	$Fo_{88.9}$ (48.1% MgO) Equil Liquid: 15.2% MgO	47.9% MgO ($Fo_{88.7}$) Equil Liquid: 14.9% MgO	15.0% MgO	1400	1570
Olova Hills	15.5% MgO	-	-	15.5% MgO	1410	1590
Myandukha Hills	13.8% MgO	-	-	13.8% MgO	1380	1540
Vinela Dike	-	$Fo_{89.5}$ (48.5% MgO) Equil Liquid: 17.0% MgO	48.7% MgO ($Fo_{89.9}$) Equil Liquid: 17.6% MgO	17.3% MgO	1440	1630

OCL - olivine control line

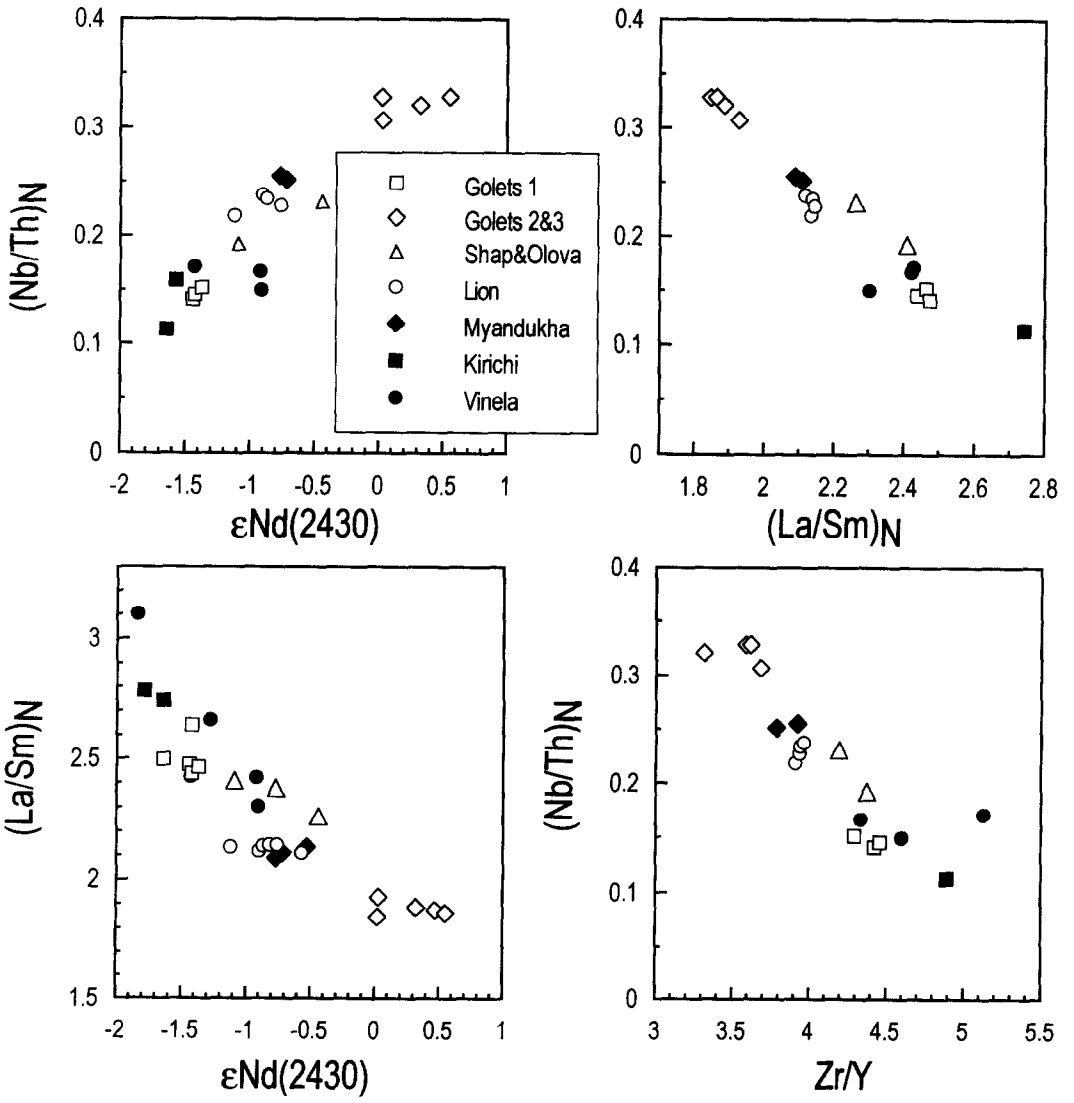

Fig. 8. Diagrams for some element ratios in the Vetreny Belt rocks.

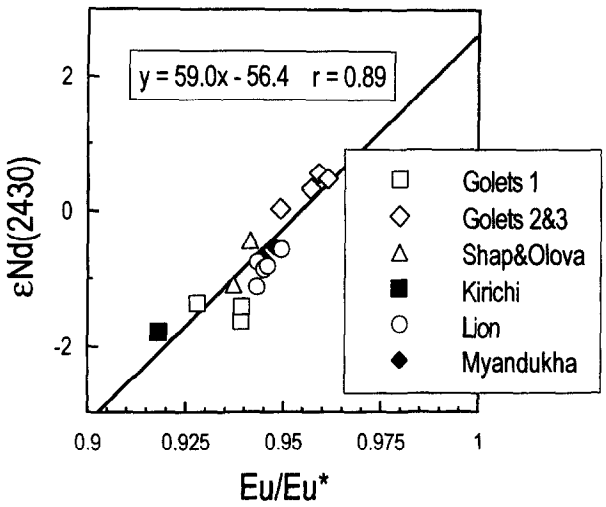

Fig. 9. Diagram Eu/Eu* vs. εNd(2430) for the Vetreny Belt rocks with results of regression line calculations.

rocks. The estimated degrees of contamination are consistent for different trace element and isotope ratios and range from ~4% for the least affected Golets flows 2 and 3 lavas to 10–12% for the Kirichi and Golets flow 1 rocks. For the Vinela Dike, the degree of contamination varies between 8 and 15%. As can be seen in Fig. 10, even 1–2% contamination results in a drastic change in Nb/Th and Nb/La ratios in a primary komatiite magma. Whereas the trace element and isotope signatures are strongly altered by assimilation, the major element compositions are not changed significantly (Table 7).

The lavas are characterized by variable CaO, TiO_2, Nb, and V, but have nearly uniform Al_2O_3, Y, and HREE abundances at a given MgO content. These relationships cannot be explained by contamination, as the most contaminated rocks show relatively elevated both Nb and La-Th-U concentrations (Fig. 2). It is also very unlikely that these differences are ascribed to the variations in mantle source compositions, because the largest differences are established for the lavas from the same locality (i.e., Golets Hills). We interpret these as a result of various degrees of partial melting. Golets flows

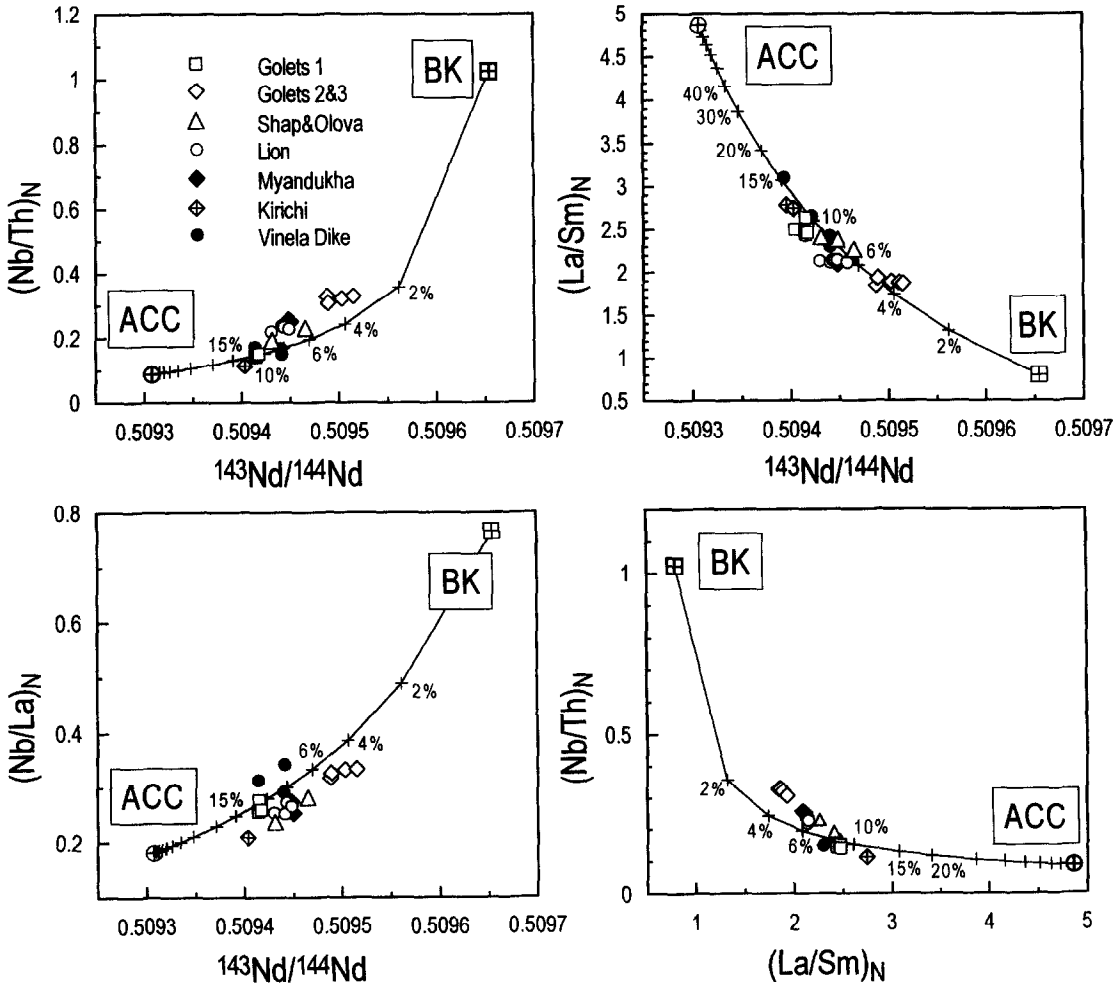

Fig. 10. Diagrams $(Nb/Th)_N$, $(La/Sm)_N$, $(Nb/La)_N$ vs. $^{143}Nd/^{144}Nd$ and $(Nb/Th)_N$ vs. $(La/Sm)_N$ for the Vetreny Belt rocks. BK-Belingwe komatiite (Chauvel et al., 1993), ACC-average Archean continental crust after Rudnick and Fountain (1995).

Table 7. Results of mixing calculations for major elements

	BK	2%	4%	6%	8%	10%	20%	30%	40%	ACC
SiO_2	49.65	50.07	50.48	50.90	51.32	51.74	53.82	55.91	57.99	70.50
TiO_2	0.430	0.429	0.429	0.428	0.428	0.427	0.424	0.421	0.418	0.400
Al_2O_3	9.01	9.12	9.23	9.33	9.44	9.55	10.09	10.63	11.17	14.40
FeO	11.74	11.57	11.39	11.22	11.05	10.88	10.01	9.15	8.28	3.10
MgO	17.59	17.26	16.93	16.60	16.27	15.94	14.29	12.64	10.99	1.10
CaO	8.79	8.67	8.55	8.43	8.31	8.19	7.59	6.99	6.39	2.80
CaO/Al_2O_3	0.976	0.951	0.927	0.903	0.880	0.858	0.753	0.658	0.573	0.194
Al_2O_3/TiO_2	20.95	21.23	21.51	21.80	22.08	22.36	23.79	25.24	26.71	36.00

BK - Belingwe komatiite; ACC - Archean continental crust

2 and 3 are enriched in CaO and TiO_2 relative to Golets flow 1 and the lava lake and probably formed by somewhat smaller degrees of partial melting, with slightly higher proportion of clinopyroxene remaining in the residue.

5.3. Sm-Nd, Pb-Pb, and U-Pb Zircon Isotope Data and the Age of the Vetreny Belt

The mineral Sm-Nd isochron ages of 2449 ± 35 and 2410 ± 34 Ma provide reliable estimates for the time of accumulation of the Vetreny suite and for the final stages of magmatism in the Vetreny Belt. The whole rock samples reveal a very narrow range in isotope compositions and Sm/Nd ratios within the single differentiated lava units implying that the erupted melts in each particular area were chemically homogeneous and have not experienced contamination after emplacement onto the surface. The age of the lavas is identical to the Sm-Nd age of the Vinela intrusion (2430 ± 174 Ma), and they have similar geochemical and isotope compositions. These similarities imply that the Vinela intrusion may represent a magma chamber feeding the Vetreny Belt volcanic rocks. On the other hand, the studied rocks are also similar in age to abundant layered intrusions in the Baltic Shield. These intrusions are documented in the Kola Peninsula, within the Belomorian Block, and in the northern and central parts of the Karelian granite greenstone terrane and are host to PGE, Cu-Ni, and Fe-Ti-V ore deposits (Turchenko, 1992). They range in age between 2470 and 2440 Ma (Fig. 11) based on U-Pb zircon and baddeleyite data and Sm-Nd isotope studies of primary minerals, and have $\epsilon Nd(T)$ values ranging between +1 and −3 (Huhma et al., 1990; Balashov et al., 1993; Bogdanova and Bibikova, 1993; Amelin et al., 1995; Amelin and Semenov, 1996). These intrusions probably also have a related origin to the Vetreny Belt volcanic and plutonic rocks.

The linear correlation in Fig. 5d represents a mixing line between two isotopically distinct endmembers: a primitive komatiite magma and material of the Archean continental crust. The calculated apparent age of 3027 ± 84 Ma is 600 Ma too old and has no geochronological significance. A similar isochron has been reported for the Kambalda volcanic rocks (Chauvel et al., 1985). In both cases the anomalously old ages obtained are attributed to the fact that the lavas had variable initial ϵNd values at the time of eruption (between −2 and +4 for Kambalda and −2 and +0.6 for the Vetreny rocks).

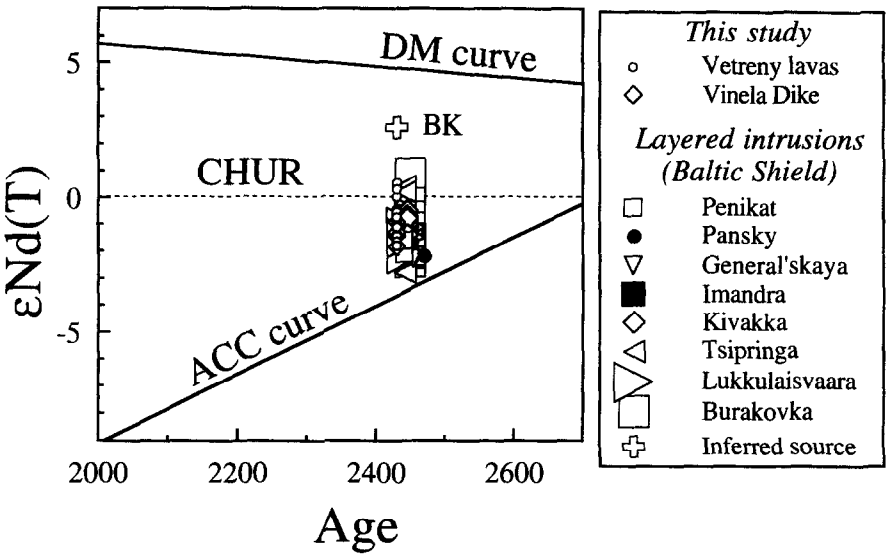

Fig. 11. Diagram $\epsilon Nd(T)$ vs. age for the Vetreny Belt rocks and layered intrusions within the Baltic Shields (Huhma et al., 1990; Balashov et al., 1993; Amelin et al., 1995; Amelin and Semenov, 1996). The Nd-parameters for DM were adopted from DePaolo and Wasserburg (1979), and those of CHUR-from Jacobsen and Wasserburg (1980, 1984); ACC-average composition of the Archean upper crust in the Vodla and Belomorian Blocks.

The Pb-Pb isochron age of 2424 ± 178 Ma agrees well with the Sm-Nd isotope data and is thought to correspond to the time of emplacement of the lavas. However, the type of event reflected by this isochron still requires explanation. Crystallization processes governing differentiation of komatiitic and basaltic magmas do not fractionate U/Pb ratios to any degree sufficient to obtain an isochron as is evident from generally unfractionated incompatible trace element ratios within each lava unit (Fig. 8). Dupré et al. (1984) attributed the large variations of U/Pb ratios in samples from the Alexo komatiite flow in Ontario to leaching of lead during secondary alteration, which is possibly also the case for the Golets flow 1. The basaltic rather than komatiitic composition and the large (45 m) thickness of the flow made it probably more resistant to secondary processes, which in turn caused smaller changes in U/Pb ratios during alteration and produced a narrower range of lead isotope ratios compared to the Alexo flow.

Another question which has to be answered concerns the significance of the calculated μ_1, or the time-integrated $^{238}U/^{204}Pb$ value of the volcanic rocks. The Golets flow 1 lavas have high μ_1 of 9.3 (compared to 8.4–8.7 in uncontaminated Abitibi and Kostomuksha komatiites; Dupré et al., 1984; Dupré and Arndt, 1990; Carignan et al., 1995; Puchtel et al., 1996a) and contain 2–5 ppm Pb, concentrations which are about an order of magnitude higher than those in uncontaminated komatiites with similar MgO content. In addition, the rocks studied are characterized by strong positive Pb-anomalies (Fig. 4). Assuming that the crustal rocks contained ~17 ppm Pb (Rudnick and Fountain, 1995), it can be shown that some 90% of the Pb in Golets flow 1 were inherited from the contaminant, and thus the lead isotope compositions of these volcanic rocks are dominated by the old upper crustal lead. The calculated $^{232}Th/^{238}U$ ratio of 4.9 ± 0.3 is close to those of 4.7 ± 0.1 determined in the lavas directly by ICP-MS (Table 2). It is substantially higher than the 4.0 value inferred for the bulk Earth (Hofmann, 1988) and probably reflects the high Th/U ratio of ~8 in the continental crust (Rudnick and Fountain, 1995).

As far as the lowermost Kirichi suite has a U-Pb zircon age of 2437 ± 3 Ma, and the uppermost Vetreny suite has the mean Sm-Nd and Pb-Pb isochron age of 2430 Ma, we conclude that the eruption rates were high, and the formation of the whole 4–8 km thick sequence was completed within several million years at the Archean-Proterozoic boundary. This high accumulation rate provides additional evidence for the proposed plume model of the formation of the Vetreny Belt, similar to the rapid eruption of plume-initiated continental flood basalts (e.g., Renne and Basu, 1991).

In summary, the Pb and to a lesser extent the neodymium isotope systems were affected by crustal contamination and do not provide direct information on the composition of the mantle source for the Vetreny Belt lavas. However, the above discussion and the modeling strongly suggest that the parental magmas to the volcanic rocks were derived from a mantle source with long-term depleted isotope and trace element signatures. Therefore, the Vetreny Belt lavas and contemporaneous mafic-ultramafic layered intrusions represent a substantial contribution of Paleoproterozoic juvenile mantle material to the existing Archean continental crust in the Baltic Shield.

5.4. Probable Tectonic Setting of the Vetreny Belt and the Significance of the 2.45 Ga Magmatic Event

2.4–2.5 Ga mafic volcanic and intrusive rocks of the Baltic Shield are part of the worldwide igneous activity indicated by layered intrusions and mafic dike swarms of similar age in other ancient cratons, i.e., the Jimberlana intrusion in Australia, the Great Dike in Zimbabwe, the Scourie picrite suite in Scotland, East Bull Lake intrusion in Ontario, and the Vestfold Hills and Napier Complex dike swarms in Antarctica (Alapieti et al., 1990). Within the Baltic Shield, about forty major and a great number of minor mafic-ultramafic intrusions are documented (Balashov et al., 1993). These intrusions constitute two extensive belts. The northern belt is located in the Kola region where it forms a chain of individual massifs along the contact between the late Archean gneisses and the early Proterozoic sequence of volcanic and sedimentary rocks of the Polmak-Pechenga-Imandra-Varzuga belt. The southern belt of intrusions is located in Finland and central and northern Karelia.

Though the Baltic Shield intrusions are more or less well-studied geologically, the composition of their parental magmas is still the subject of debate. For some intrusions, a boninitic parental magma has tentatively been proposed (see discussion in Alapieti et al., 1990). We consider this misleading because boninites are rare high-MgO and compatible- and moderately-incompatible (e.g., HREE) element enriched basalts, which are normally regarded as being diagnostic of particular conditions in oceanic arc settings (Murton, 1989; Taylor et al., 1994).

We argue that the Vetreny Belt lavas and the contemporaneous layered intrusions in central and northern Karelia had a similar parental magma. This magma is inferred to have had a komatiitic composition and was generated in a mantle plume. Impinging of a plume head beneath the continental lithosphere resulted in its elevation and placed it under tension. The significance of the tension was that it led to the lithosphere thinning, stretching, and rifting (Hill, 1991), but did not go as far as to cause the continental breakup and opening of a new ocean. We argue that these komatiite magmas have been emplaced in continental rift setting because the accompanying sediments are largely terrigenous and most volcanic rocks appear to occur in graben-like structures. The lack of vast volumes of felsic intrusive magmatism between 2.4–2.5 Ga in the Baltic Shield also implies that no large-scale crustal growth by accretion in an arc system occurred.

6. CONCLUSIONS

The Vetreny Belt lavas and the Vinela Dike had a related origin and constitute a single volcano-plutonic association. The MgO contents of the erupted and intruded magmas suggest that the liquidus temperatures increased from 1370 to 1440°C towards the center of the Vetreny Belt. The source of the magmas had a potential temperature at least 150°C higher than the ambient mantle. This consideration together with a steep thermal gradient beneath the Vetreny Belt are evidence for the existence of a mantle plume underlying the southeastern Baltic Shield at ~2.45 Ga.

The parental magmas to the lavas and the Vinela Dike had a komatiite composition and were derived from a long-

term LREE and other highly incompatible trace element depleted mantle source with $\epsilon Nd(T)$ of ca. +2.6. The evolution of these magmas was mainly controlled by 4–15% contamination with felsic crustal rocks both en route to the surface and in intermediate magma chambers, which resulted in substantial changes in trace element and isotope ratios.

The Sm-Nd internal isochron ages of 2.41–2.44 Ga, a bulk-rock Pb-Pb age of 2.42 Ga, and a U-Pb zircon age of 2437 ± 3 Ma for the lavas and the Vinela Dike are identical to the published U-Pb zircon and baddeleyite ages of 2.44–2.47 Ga for layered mafic-ultramafic intrusions in the southeastern Baltic Shield. Based on the chemical and isotope similarities between the lavas and the intrusions, we conclude that they had allied parental magmas.

The vast volumes of these parental komatiite magmas were emplaced in continental rift setting during interaction of a mantle plume and continental crust. Impinging of a plume head beneath the continental lithosphere resulted in its thinning, stretching, and rifting but failed to open a new ocean. The 2.45 Ga magmatic event resulted in a substantial addition of new juvenile mantle material to the existing Archean continent in the Baltic Shield.

Acknowledgments—V. Kevlich, N. Ashikhmina, and V. Pavlichenko did a bang-up job of obtaining the mineral separates and handpicking. Discussions with Yu. Amelin, A. Shchipansky, A. Girnis, S. Bogdanova, and K. Mezger and reviews by C. Herzberg and E. Nisbet substantially improved the initial draft of the manuscript. This study was supported by an Alexander von Humboldt fellowship to I. Puchtel and by the Russian Foundation for Fundamental Research.

Editorial handling: M. Menzies

REFERENCES

Abbott D. (1996) Plumes and hotspots as sources of greenstone belts. *Lithos* **37,** 113–127.

Abbott D. and Mooney W. (1995) The structural and geochemical evolution of the continental crust: Support for the oceanic plateau model of continental growth. *IUGG Nat. Rep.* 231–242.

Abbott D., Burgess L., Longhi J., and Smith W. H. F. (1994) An empirical thermal history of the Earth's upper mantle. *J. Geophys. Res.* **99,** 13835–13850.

Alapieti T. T., Filen B. A., Lahtinen J. J., Lavrov M. M., Smolkin V. F., and Voitsekhovsky S. N. (1990) Early Proterozoic layered intrusions in the northeastern part of the Fennoscandian Shield. *Mineral. Petrol.* **42,** 1–22.

Amelin Yu. V. and Semenov V. S. (1996) Neodymium and strontium isotopic geochemistry of mafic layered intrusions in the eastern Baltic Shield: Implications for the evolution of Paleoproterozoic continental mafic magmas. *Contrib. Mineral. Petrol.* **124,** 255–272.

Amelin Yu. V., Heaman L. M., and Semenov V. S. (1995) U-Pb geochronology of layered mafic intrusions in the eastern Baltic Shield: Implications for the timing and duration of Paleoproterozoic continental rifting. *Precambrian Res.* **75,** 31–46.

Arndt N. T. (1986) Komatiites: A dirty window to the Archean mantle. *Terra Cognita* **6,** 59–66.

Arndt N. T. and Goldstein S. L. (1989) An open boundary between lower continental crust and mantle: Its role in crust formation and crust recycling. *Tectonophysics* **161,** 201–212.

Arndt N. T. and Jenner G. A. (1986) Crustally contaminated komatiites and basalts from Kambalda, Western Australia. *Chem. Geol.* **56,** 229–255.

Balashov Yu. A., Bayanova T. B., and Mitrofanov F. P. (1993) Isotope data on the age and genesis of layered basic-ultrabasic intrusions in the Kola Peninsula and northern Karelia, northeastern Baltic Shield. *Precambrian Res.* **64,** 197–205.

Bau M. (1991) Rare-earth element mobility during hydrothermal and metamorphic fluid-rock interaction and the significance of the oxidation state of europium. *Chem. Geol.* **93,** 219–230.

Beattie P., Ford C., and Russell D. (1991) Partition coefficients for olivine-melt and orthopyroxene-melt systems. *Contrib. Mineral. Petrol.* **109,** 212–224.

Bibikova E. V., Skiöld T., and Bogdanova S. V. (1996) Age and geodynamic aspects of the oldest rocks in the Precambrian Belomorian Belt of the Baltic (Fennoscandian) Shield. *Geol. Soc. London, Spec. Publ.* **112,** 55–67.

Bogdanova S. V. and Bibikova E. V. (1993) The Saamian of the Belomorian Mobile Belt: New geochronological constraints. *Precambrian Res.* **64,** 131–152.

Brandon A. D., Hooper P. R., Goles G. G., and Lambert R. S. J. (1993) Evaluating crustal contamination in continental basalts: The isotopic composition of the Picture Gorge Basalt of the Columbia River Basalt Group. *Contrib. Mineral. Petrol.* **114,** 452–464.

Carignan J., Machado N., and Gariépy C. (1995) U-Pb isotopic geochemistry of komatiites and pyroxenes from the southern Abitibi greenstone belt, Canada. *Chem. Geol.* **126,** 17–27.

Chauvel C., Dupré B., and Jenner G. A. (1985) The Sm-Nd age of Kambalda volcanics is 500 Ma too old! *Earth Planet. Sci. Lett.* **74,** 315–324.

Chauvel C., Dupré B., and Arndt N. T. (1993) Pb and Nd isotope correlation in Belingwe komatiites and basalts. In *The Geology of the Belingwe Greenstone Belt, Zimbabwe. A Study of the Evolution of Archaean Continental Crust* (ed. M. J. Bickle and E. G. Nisbet), pp. 167–174. A. A. Balkema.

Compston W., Williams I. S., Campbell I. H., and Gresham J. J. (1986) Zircon xenocrysts from the Kambalda volcanics: Age constraints and direct evidence for older continental crust below the Kambalda-Norseman greenstones. *Earth Planet. Sci. Lett.* **76,** 299–311.

DePaolo D. J. and Wasserburg G. J. (1979) Sm-Nd age of the Stillwater Complex and the mantle evolution curve for neodymium. *Geochim. Cosmochim. Acta* **43,** 999–1008.

Desrochers J.-P., Hubert C., Ludden J. N., and Pilote P. (1993) Accretion of Archaean oceanic plateau fragments in the Abitibi greenstone belt, Canada. *Geology* **21,** 451–454.

Dupré B. and Arndt N. T. (1990) Lead isotopic composition of Archean komatiites and sulfides. *Chem. Geol.* **85,** 35–56.

Dupré B., Chauvel C., and Arndt N. T. (1984) Lead and Neodymium isotopic study of two Archean komatiitic flows from Alexo, Ontario. *Geochim. Cosmochim. Acta* **48,** 1965–1972.

Evensen N. M., Hamilton P. J., and O'Nions R. K. (1978) Rare earth element abundances in chondritic meteorites. *Geochim. Cosmochim. Acta* **42,** 1199–1212.

Farnetani C. G. and Richards M. A. (1994) Numerical investigations of the mantle plume initiation model for flood basalt events. *J. Geophys. Res.* **99,** 13813–13833.

Fletcher I. R. and Rosman K. J. R. (1982) Precise determination of initial ϵNd from Sm-Nd isochron data. *Geochim. Cosmochim. Acta* **46,** 19–22.

Gaál G. and Gorbatschev R. (1987) An outline of the Precambrian evolution of the Baltic Shield. *Precambrian Res.* **35,** 15–52.

Garbe-Schönberg C.-D. (1993) Simultaneous determination of thirty-seven trace elements in twenty-eight international rock standards by ICP-MS. *Geostand. Newslett.* **17,** 81–97.

Green T. H. (1994) Experimental studies of trace-element partitioning applicable to igneous petrogenesis-Sedona 16 years later. *Chem. Geol.* **117,** 1–36.

Glazner A. F. and Farmer G. L. (1992) Production of isotopic variability in continental basalts by cryptic crustal contamination. *Science* **255,** 72–74.

Gorbatschev R. and Bogdanova S. V. (1993) Frontiers in the Baltic Shield. *Precambrian Res.* **64,** 3–21.

Hanson G. N. and Langmuir C. H. (1978) Modeling of major elements in mantle-melt systems using trace element approaches. *Geochim. Cosmochim. Acta* **42,** 725–741.

Hart S. R. and Zindler A. (1986) In search for bulk-earth composition. *Chem. Geol.* **57,** 247–267.

Hawkesworth C. J., Marsh J. S., Duncan A. R., Erlank A. J., and Norry M. J. (1984) The role of continental lithosphere in the

generation of the Karoo volcanic rocks: evidence from combined Nd- and Sr-isotope studies. *Geol. Soc. S. Afr., Spec. Publ.* **13,** 341–354.

Hawkesworth C. J., Mantovani M., and Peate D. (1988) Lithosphere remobilization during Parana CFB magmatism. *J. Petrol., Spec. Lithosphere Issue,* 205–223.

Herzberg C. (1995) Generation of plume magmas through time: An experimental perspective. *Chem. Geol.* **126,** 1–16.

Hill R. E. T. (1991) Starting plumes and continental break-up. *Earth Planet. Sci. Lett.* **104,** 398–416.

Hoffman P. F. (1990) On accretion of granite-greenstone terranes. In *Greenstone Gold and Crustal Evolution, Val D'Or, Canada* (ed. F. Robert), pp. 32–45. Geol. Assoc. Canada Mineral Deposits Div.

Hofmann A. W. (1988) Chemical differentiation of the Earth: The relationship between mantle, continental crust, and oceanic crust. *Earth Planet. Sci. Lett.* **90,** 297–314.

Huhma H., Cliff R. A., Perttunen V., and Sakko M. (1990) Sm-Nd and lead isotopic study of mafic rocks associated with Early Proterozoic continental rifting: The Perapohja schist belt in northern Finland. *Contrib. Mineral. Petrol.* **104,** 369–379.

Huppert H. E. and Sparks R. S. J. (1985) Cooling and contamination of mafic and ultramafic magmas during ascent through continental crust. *Earth Planet. Sci. Lett.* **74,** 371–386.

Huppert H. E., Sparks R. S. J., Turner J. S., and Arndt N. T. (1984) Emplacement and cooling of komatiite lavas. *Nature* **309,** 19–22.

Jacobsen S. B. and Wasserburg G. J. (1980) Sm-Nd isotopic evolution of chondrites. *Earth Planet. Sci. Lett.* **50,** 139–155.

Jacobsen S. B. and Wasserburg G. J. (1984) Sm-Nd isotopic evolution of chondrites and achondrites, II. *Earth Planet. Sci. Lett.* **67,** 137–150.

Jochum K. P., Arndt N. T., and Hofmann A. W. (1991) Nb-Th-La in komatiites and basalts: Constraints on komatiite petrogenesis and mantle evolution. *Earth Planet. Sci. Lett.* **107,** 272–289.

Kimura G., Ludden J. N., Desrochers J.-P., and Hori R. (1993) A model of ocean-crust accretion for the Superior province, Canada. *Lithos* **30,** 337–355.

Krogh T. E. (1982) Improved accuracy of U-Pb zircon ages by the creation of more concordant systems using an air abrasion technique. *Geochim. Cosmochim. Acta* **46,** 637–649.

Kulikov V. S. (1983) The Proterozoic. In *The Earth's Crust and Metallogeny in the Southeastern Part of the Baltic Shield* (ed. K. O. Krats), pp. 32–40. Nauka.

Kulikov V. S. (1988) High-magnesian volcanism in the early Proterozoic. In *Komatiites and High-Magnesian Volcanics in the Early Precambrian of the Baltic Shield* (ed. O. A. Bogatikov), pp. 20–88. Nauka.

Kulikov V. S. et al. (1990) Evolution of Archaean magmatism in the Vodla Block, Karelian granite-greenstone terrane. In *Precambrian Geology and Geochronology of the East European Platform* (ed. S. B. Lobach-Zhuchenko and E. V. Bibikova), pp. 92–100. Nauka.

Lobach-Zhuchenko S. B., Chekulaev V. P., Sergeev S. A., Levchenkov O. A., and Krylov I. N. (1993) Archaean rocks from southeastern Karelia (Karelian granite-greenstone terrain). *Precambrian Res.* **62,** 375–397.

Ludwig K. R. (1992) ISOPLOT—a plotting and regression program for radiogenic - isotope data, version 2.57. US Geol. Survey Open-File Rep. 91-445.

Luosto U., Flueh E., and Lund C. (1989) The crustal structure along the POLAR profile from seismic refraction investigations. *Tectonophysics* **162,** 51–85.

Manhès G., Minster J. F., and Allegre C. J. (1978) Comparative uranium-thorium-lead and rubidium-strontium of Saint Severine amphoterite: Consequences for Early solar system chronology. *Earth Planet. Sci. Lett.* **39,** 14–24.

McDonough W. F. (1990) Constraints on the composition of the continental lithospheric mantle. *Earth Planet. Sci. Lett.* **101,** 1–18.

McDonough W. F. and Sun S.-S. (1995) The composition of the Earth. *Chem. Geol.* **120,** 223–253.

McKenzie D. and Bickle M. J. (1988) The volume and composition of melt generated by extension of the lithosphere. *J. Petrol.* **29,** 625–679.

Michard A. and Albarède F. (1986) The REE content of some hydrothermal fluids. *Chem. Geol.* **55,** 51–60.

Murton B. J. (1989) Tectonic controls on boninite genesis. In *Magmatism in the Ocean Basins* (ed. A. D. Saunders and M. J. Norry); *Geol. Soc. Spec. Publ. No.* **42,** 347–377.

Nemchin A. A., Pidgeon R. T., and Wilde S. A. (1994) Timing of Late Archaean granulite facies metamorphism in the southwestern Yilgarn Craton of Western Australia: Evidence from U-Pb ages of zircons from mafic granulites. *Precambrian Res.* **68,** 307–321.

Nisbet E. G. et al. (1987) Uniquely fresh 2.7 Ga komatiites from the Belingwe greenstone belt, Zimbabwe. *Geology* **15,** 1147–1150.

Nisbet E. G., Cheadle M. J., Arndt N. T., and Bickle M. J. (1993) Constraining the potential temperature of the Archaean mantle: A review of the evidence from komatiites. *Lithos* **30,** 291–307.

Puchtel I. S., Zhuravlev D. Z., Kulikov V. S., and Kulikova V. V. (1991) Petrography and Sm-Nd age of a differentiated komatiitic basalt lava flow in the Vetreny belt, Baltic Shield. *Geochem. Int.* **28,** 14–23.

Puchtel I. S., Hofmann A. W., Jochum K. P., Mezger K., Shchipansky A. A., and Samsonov A. V. (1996a) The Kostomuksha greenstone belt, N.W. Baltic Shield: Remnant of a late Archean oceanic plateau? *Terra Nova* (submitted).

Puchtel I. S., Hofmann A. W., Mezger K., Shchipansky A. A., Kulikov V. S., and Kulikova V. V. (1996b) Petrology of a 2.41 Ga remarkably fresh komatiitic basalt lava lake in Lion Hills, central Vetreny Belt, Baltic Shield. *Contrib. Mineral. Petrol.* **124,** 273–290.

Renne P. R. and Basu A. R. (1991) Rapid eruption of the Siberian Traps flood basalts at the Permo-Triassic boundary. *Science* **253,** 176–179.

Richards M. A., Duncan R. A., and Courtillot V. E. (1989) Flood basalts and hot-spot tracks: Plume heads and tails. *Science* **246,** 103–107.

Richter F. M. (1988) A major change in the thermal state of the Earth at the Archean-Proterozoic boundary: Consequences for the nature and preservation of continental lithosphere. *J. Petrol., Spec. Lithosphere Issue,* 39–52.

Roeder P. L. and Emslie R. F. (1970) Olivine-liquid equilibrium. *Contrib. Mineral. Petrol.* **29,** 275–282.

Rudnick R. L. and Fountain D. M. (1995) Nature and composition of the continental crust: A lower crustal perspective. *Rev. Geophys.* **33,** 267–309.

Ryabchikov I. D., Suddaby P., Girnis A. V., Kulikov V. S., Kulikova V. V., and Bogatikov O. A. (1988) Trace-element geochemistry of Archean and Proterozoic rocks from eastern Karelia, USSR. *Lithos* **21,** 183–194.

Sokolov V. A. (1987) *Geology of Karelia.* Nauka.

Tatsumoto M., Knight R. J., and Allegre C. J. (1973) Time differences in the formation of meteorites as determined from the ratio of lead 207 to lead 206. *Science* **180,** 1279–1283.

Taylor R. N., Nesbitt R. W., Vidal P., Harmon R. S., Auvray B., and Croudace I. W. (1994) Mineralogy, chemistry, and genesis of the boninite series volcanics, Chichijima, Bonin-Islands, Japan. *J. Petrol.* **35,** 577–617.

Thirlwall M. F. (1982) A triple-filament method for rapid and precise analysis of rare earth elements by isotope dilution. *Chem. Geol.* **35,** 155–166.

Timmerman M. J. and Daly J. S. (1995) Sm-Nd evidence for late Archaean crust formation in the Lapland-Kola Mobile Belt, Kola Peninsula, Russia and Norway. *Precambrian Res.* **72,** 97–107.

Turchenko S. I. (1992) Precambrian metallogeny related to tectonics in the eastern part of the Baltic Shield. *Precambrian Res.* **58,** 121–141.

Watson S. and McKenzie D. (1991) Melt generation by plumes: A study of Hawaiian volcanism. *J. Petrol.* **32,** 501–537.

White R. S. and McKenzie D. (1995) Mantle plumes and flood basalts. *J. Geophys. Res.* **100,** 17543–17585.

York D. (1966) Least squares fitting of straight line. *Canadian J. Phys.* **44,** 1079–1086.

York D. (1969) Least squares fitting of a straight line with correlated errors. *Earth Planet. Sci. Lett.* **5,** 320–324.

Zhuravlev D. Z., Puchtel I. S., and Samsonov A. V. (1989) Sm-Nd age and geochemistry of metavolcanics from the Olondo greenstone belt, Aldan Shield. Izv. AN SSSR. *Ser. Geol.* **2,** 39–49.